ESTIMATING NEURAL CURRENTS FROM

NEUROMAGNETIC MEASUREMENTS

Kimmo Uutela

ESTIMATING NEURAL CURRENTS FROM

NEUROMAGNETIC MEASUREMENTS

Kimmo Uutela

Brain Research Unit, Low Temperature Laboratory,
Helsinki University of Technology

Title: Estimating neural currents from neuromagnetic measurements

Author: Kimmo Uutela
              Brain Research Unit, Low Temperature Laboratory
              Helsinki University of Technology
              P.O. Box 2200, 02015 HUT, FINLAND
              Kimmo.Uutela@hut.fi

Abstract: This thesis concerns three new methods for estimating the electrical activity of the human brain from the magnetic fields measured outside the head. The first method models the electrical activity as a combination of focal current dipoles and applies global optimization to estimate their locations without need for an initial solution. The second method is the minimum current estimate that is capable of modeling both focal and distributed electrical activity. The third method measures the movements of the head during the measurements and uses this information for more accurate estimates of the neural currents. The usability of the methods is demonstrated using simulations and measurements. The minimum current estimate is also applied to four experiments of cognitive processes in the human brain: one studying visuomotor interaction, second studying visual attention, third studying integration of auditory and visual representations of letters, and fourth studying observation of sign language in signing and non-signing subjects.

Estimating neural currents from neuromagnetic measurements

Author: Kimmo Uutela
                           Brain Research Unit,
                           Low Temperature Laboratory,
                           Helsinki University of Technology

Publications

The dissertation consists of the present summary article and the following papers:

P1 Uutela, K., Hämäläinen, M., and Salmelin, R. (1998). Global optimization in the localization of neuromagnetic sources. *IEEE Trans. Biomed. Eng.*, 45:716–723.

P2 Uutela, K., Hämäläinen, M., and Somersalo, E. (1999). Visualization of magnetoencephalographic data using minimum current estimates. *NeuroImage*, 10:173–180.

P3 Uutela, K., Taulu, S., and Hämäläinen, M. (2001). Detecting and correcting for head movements in neuromagnetic measurements. *NeuroImage*, 14:1424–1431.

P4 Nishitani, N., Uutela, K., Shibasaki, H., and Hari, R. (1999). Cortical visuomotor integration during eye pursuit and eye–finger pursuit. *J. Neurosci.*, 19:2647–2657.

P5 Vanni, S. and Uutela, K. (2000). Foveal attention modulates responses to peripheral stimuli. *J. Neurophys.*, 83:2443–2452.

P6 Raij, T., Uutela, K., and Hari, R. (2000). Audiovisual integration of letters in the human brain. *Neuron*, 28:617–625.

P7 Levänen, S., Uutela, K., Salenius, S., and Hari, R. (2001). Cortical representation of sign language: Comparison of deaf signers and hearing non-signers. *Cerebral Cortex*, 11:506–512.

Contributions of the author

I was the principal author in publications P1–P3. I designed the methods in P1 and the correction methods in P3; I made improvements based on work of other authors on the methods in P2 and the measurement methods in P3. The neuromagnetic data used as an example in P1 and P2 were adopted from other studies; the data in P3 were measured together with the other authors. I implemented most of the methods, carried out the simulations, and analyzed the data. I wrote most of the manuscripts P1–P3, but other authors participated actively.

In publications P4–P7 the experimental setups were mainly suggested by the principal authors; I suggested some of the control measurements in P5. I generated, together with the principal author, the stimuli in publications P4 and P7 and the control measurements for P5. I participated in the measurements only in the controls of P5. I had a major contribution to the data analysis in publications P5, P6, and P7 and a small contribution in P4. In publications P4–P7 the principal author was responsible for writing the manuscript, but I participated actively with the other coauthors.

Table of contents

Abbreviations

BEM	Boundary element model
EEG	Electroencephalography
FC	Forward calculation
FDM	Finite difference method
FEM	Finite element model
FEF	Frontal eye field
FIR	Finite impulse response
fMRI	Functional magnetic resonance imaging
MCE	Minimum current estimate
MEG	Magnetoencephalography
MNE	Minimum-norm estimate
MUSIC	Multiple signal classification
PET	Positron emission tomography
ROI	Region of interest
SPM	Statistical parameter map
SQUID	Superconducting quantum interference device
SSP	Signal-space projection
STS	Superior temporal sulcus

Preface

This thesis work was carried out in the Brain Research Unit of the Low Temperature Laboratory at the Helsinki University of Technology. The work was financially supported by the Academy of Finland, the Helsinki University of Technology, Jenny and Antti Wihuri Foundation, and the Finnish Graduate School of Neuroscience.

The facilities and general attitude in the laboratory have provided opportunities for working at the vanguard of the research of ultralow temperature physics and neuromagnetic brain studies, and this is largely due to the efforts of its first director, Academician Olli V. Lounasmaa, and his follower, Prof. Mikko Paalanen.

The major force driving the Brain Research Unit has been Prof. Riitta Hari. I have not seen similar ability to master, on one hand, both the administrative and scientific sides, and on the other hand, both the neuroscientific and methodological sides of the work done in the unit.

My supervisor, Doc. Matti Hämäläinen, has had wide experience and insight into the neuromagnetic data analysis methods, which has been invaluable for the work I have done. I am also grateful to Doc. Riitta Salmelin for her guidance when I started my work with neuromagnetic measurements, and to Prof. Erkki Somersalo, whose work has been the basis for the most extensively applied method in this study.

It has been a pleasure working also with my other coauthors, Dr. Sari Levänen, Dr. Nobuyuki Nishitani, Dr. Tommi Raij, Dr. Stephan Salenius, Prof. Hiroshi Shibasaki, Mr. Samu Taulu, and Dr. Simo Vanni.

I wish to thank my supervising professor, Prof. Raimo P. Hämäläinen, for teaching how to incorporate mathematical modeling into real problems.

Considering the amount of special needs the neuromagnetic measurements pose, working in the laboratory has included surprisingly few bureaucratic and technical obstacles. This would not have been possible without the work of the secretarial and technical personnel. I am especially thankful to Lic. Marja Holmström for creating the cozy atmosphere of the laboratory. One major factor has also been the excellent equipment and support by Neuromag Ltd. and its personnel.

I am grateful to Riitta Hari and Mika Seppä for useful comments on the manuscript and to Doc. Risto Ilmoniemi and Prof. Jari Kaipio for the thorough review.

During the eight years I have been in the Low Temperature Laboratory I have enjoyed the opportunity to work with a multitude of exceptional colleagues, and I wish to thank them both for their role in my work and their role as friends.

I wish to thank Kim Simelius for serving as my big brother during our time in Otaniemi. I wish to thank Mika Seppä for being both a valuable colleague and a trusted friend. And I wish to thank Tiina Vuorinen for her contagious positiveness at some unhappy times.

I wish to thank my parents and sisters for their continuous support. Finally, I wish to thank Katri for being the most important person in my life and for surviving over ten years of our turbulent relationship.

Espoo, November 2001
Kimmo Uutela

Chapter 1

Introduction

The human brain is an extremely complex system performing demanding information processing tasks rapidly. All the cognitive processes of human beings seem to have correlates in the physiological processes of the brain, and brain injuries cause different cognitive deficits. The ways in which the brain accomplishes its tasks are largely unknown, and discovering these is presently one of the most intriguing challenges of science.

The brain consists of billions of neurons, each connected to others through thousands of synapses. This huge network has many electric and chemical processes that can be measured in various ways. Magnetoencephalography (MEG) (Cohen, 1968; Hämäläinen et al., 1993) is the study of magnetic fields generated by currents in the neurons. It can be used to non-invasively measure even the fastest activations in all parts of the cortex simultaneously. Electroencephalography (EEG) is a closely related method that measures the electric fields generated by the same neuronal currents. If precise timing of the events is not an issue, the brain functions can be studied with a better spatial resolution by measuring the changes of the blood flow or oxygenation with position emission tomography (PET) or functional magnetic resonance imaging (fMRI).

This work concentrates on MEG since it has a good temporal resolution compared with fMRI or PET and is less sensitive to anatomic differences between the heads of different subjects than EEG. The work includes both development of practical methods for estimating the neural currents and applications of the methods to studies of the human cognitive system.

Chapter 2

Magnetoencephalography

2.1   Neural currents

The membrane surrounding a neuron is not just a passive, protective sheet. Instead, it contains chemically activated ion channels and active ion pumps that change the electrical properties of the neuron.

When a neuron is not externally activated, the ion pumps maintain internal ion concentrations that differ from the concentrations outside (Kandel et al., 1991). The inside of the neuron contains more potassium (K^+) ions and clearly less sodium (Na^+) ions. The imbalance of these and some other ions cause the neuron to have a lower resting potential inside than outside; the voltage is typically -70 mV.

When an electric signal arrives at a synapse, it causes the presynaptic cell to release transmitter molecules that move to the receptors of the postsynaptic cell. This causes the related ion channels to open, which allows the concentration differences to balance. The ion channels are ion specific; if a K^+ channel opens, the K^+ flows out of the cell causing the potential to drop, whereas opening of a Na^+ channel causes the potential to increase. If the potential in the soma (cell body) increases enough, a propagating electrical impulse, an action potential, is generated in the axon activating eventually synapses at other neurons.

Most of the excitatory synapses are located in the dendritic tree far away from the soma (Fig. 2.1). When the potential in the dendrites increases, the ionic current flows both towards the tips of the dendrites and towards the cell body. When several excitatory synapses in the dendritic tree are activated, the net current in the tips of the dendrites is small due to different orientations of the dendrites, but since all the currents converge in the apical dendrite, it has an intracellular net current from the dendrites towards the cell body. Since the pyramidal neurons have similar orientations, having dendrites close to the surface and cell bodies deeper, activating several excitatory synapses of pyramidal cells usually causes a neuronal net current perpendicular to the surface of the cortex. The magnetic field produced by this current can be measured with MEG. Activation of inhibitory synapses or synapses close to the cell body can also produce measurable, although usually weaker, magnetic signals.

The transfer of ions through the neuronal membrane naturally causes potential differences also outside the neuron. These potential differences balance with ohmic currents flowing between the brain cells.
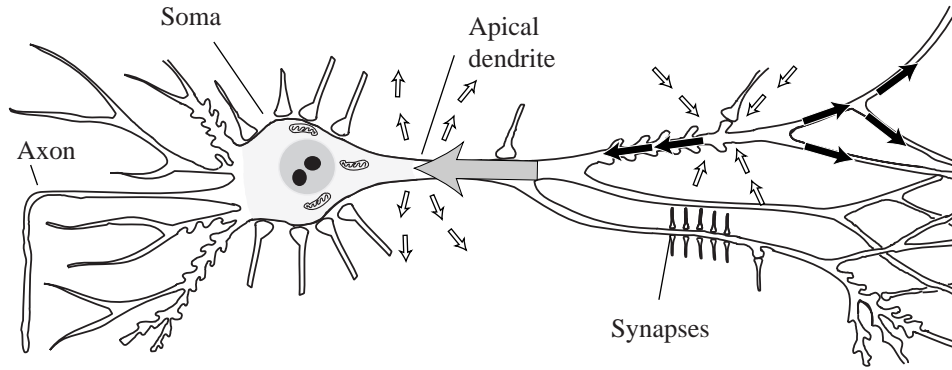
Figure 2.1: A pyramidal neuron. Activation of excitatory synapses in the dendrites cause ionic currents in the dendrites (small black arrows) that converge in the apical dendrite (gray arrow). The ionic currents through the neuronal membrane cause currents also outside the cells (white arrows). Modified from (Iversen, 1979).

2.2 Neuromagnetic fields

The electromagnetic field is governed by the Maxwell's equations:

$$\nabla \cdot \mathbf{E} \;=\; \rho/\varepsilon_0, \tag{2.1}$$
$$\nabla \times \mathbf{E} \;=\; -\partial \mathbf{B}/\partial t, \tag{2.2}$$
$$\nabla \cdot \mathbf{B} \;=\; 0, \tag{2.3}$$
$$\nabla \times \mathbf{B} \;=\; \mu_0 \left(\mathbf{J} + \varepsilon_0 \, \partial \mathbf{E}/\partial t \right), \tag{2.4}$$

where $\mathbf{E}$ and $\mathbf{B}$ are the electric and magnetic fields, $\mathbf{J}$ and ρ are the total current density and charge density, t is time, and ε_0 and μ_0 are the permittivity and permeability of the free space, respectively.

Most of the bioelectric signals are below 1 kHz frequency. Thus, on the macroscopic level, the ohmic current is larger than the effect of the changing field. Therefore, for the purpose of calculating the magnetic field at a certain time, the equations can be simplified using the quasistatic approximation that the temporal derivatives in Eq. (2.2) and Eq. (2.4) are negligible. Thus, on the macroscopic level, the electric field can be described as the gradient of an electric potential V. The magnetic field in a specified location $\mathbf{r}$ can be calculated using the Ampère-Laplace law:

$$\mathbf{B}(\mathbf{r}) = \frac{\mu_0}{4\pi} \int \frac{\mathbf{J}(\mathbf{r}') \times (\mathbf{r} - \mathbf{r}')}{\|\mathbf{r} - \mathbf{r}'\|^3} \mathrm{d}v', \tag{2.5}$$

where $\mathbf{r}'$ and $\mathrm{d}v'$ correspond to coordinates within the brain.

The currents within neurons are accompanied by ohmic currents outside. To separate these two, the volume current is defined as the ohmic current governed by the macroscopic electric potential and macroscopic conductivity σ:

$$\mathbf{J}_v = -\sigma \nabla V, \tag{2.6}$$

while the remaining part, governed mainly by the potentials and conductivities of the neuronal membrane, is called the primary current:

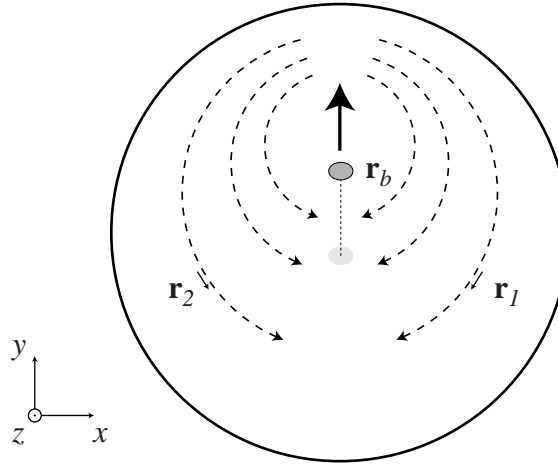$$\mathbf{J}_p = \mathbf{J} - \mathbf{J}_v. \tag{2.7}$$

Figure 2.2: Primary current (solid arrow) causes volume currents (dashed arrows) in a spherically symmetrical conductor model.

To calculate the magnetic field generated by a given distribution of the primary current, a model for the macroscopic conductivity is needed. The most generally used model for MEG is the spherically symmetrical conductor model. The exact shape of the brain can be taken into account by describing the conductivity with a piecewise homogeneous boundary element model (BEM) (Hämäläinen and Sarvas, 1989). Smaller details in the conductivity and its anisotropy can be taken into account using finite difference method (FDM) or finite element model (FEM) (Johnson, 1997; Buchner et al., 1997; Ramon et al., 2000).

One special feature of the spherical conductivity model is that only tangential components of the primary current cause magnetic fields outside the head. Assume a spherically symmetrical conductor with a current element along the y axis at location $\mathbf{r}_p = (0, y_p, 0)$, producing volume currents within the sphere (Fig. 2.2). Consider a location on the surface of the sphere in the yz-plane $\mathbf{r}_b(0, y_b, z_b)$ and the radial component of its magnetic field: $\mathbf{B}(\mathbf{r}_b) \cdot \mathbf{r}_b / \|\mathbf{r}_b\|$. The system is symmetric in relation to the reflection across the yz-plane. Therefore, if location $\mathbf{r}_1 = (x, y, z)$ has current density $\mathbf{q}_1 = (q_x, q_y, q_z)$, the mirror location $\mathbf{r}_2 = (-x, y, z)$ has mirror current density $\mathbf{q}_2 = (-q_x, q_y, q_z)$. The sum of the contributions by current elements in $\mathbf{r}_1$ and $\mathbf{r}_2$ is, according to the Ampère–Laplace law Eq. (2.5),

$$
\begin{aligned}
\mathrm{d}\mathbf{B}(\mathbf{r}_b) \cdot \frac{\mathbf{r}_b}{\|\mathbf{r}_b\|} &= \frac{\mu_0 \, \mathrm{d}v}{4\pi \|\mathbf{r}_b\| \, \|\mathbf{r}_b - \mathbf{r}_1\|^3} \\
&\quad \left(\mathbf{q}_1 \times (\mathbf{r}_b - \mathbf{r}_1) \cdot \mathbf{r}_b + \mathbf{q}_2 \times (\mathbf{r}_b - \mathbf{r}_2) \cdot \mathbf{r}_b \right) \\
&= \frac{\mu_0 \, \mathrm{d}v}{4\pi \|\mathbf{r}_b\| \, \|\mathbf{r}_b - \mathbf{r}_1\|^3} \\
&\quad \left(\begin{vmatrix} 0 & y_b & z_b \\ q_x & q_y & q_z \\ -x & y_b - y & z_b - z \end{vmatrix} + \begin{vmatrix} 0 & y_b & z_b \\ -q_x & q_y & q_z \\ x & y_b - y & z_b - z \end{vmatrix} \right) \\
&= 0.
\end{aligned} \tag{2.8}
$$

For locations in the yz-plane, including the primary current, current orientation is also

in the yz-plane. Therefore, the contribution of these currents to the magnetic field at $\mathbf{r}_b$ is perpendicular to the yz-plane and not radial, either. Due to the symmetry, the same holds for fields at any location on the surface of the sphere.

The outside of the head is assumed to have zero conductivity and therefore no electric currents. According to Eq. (2.4) and the quasistatic assumption, $\nabla \times \mathbf{B} = 0$ and the magnetic field can be described as the gradient of the magnetic scalar potential U. The potential difference of two points with distance r from the surface of the brain is the line integral of the magnetic field, which is, according to Eq. (2.5), limited:

$$|\Delta U| \leq \frac{\mu_0}{4r} \int \|\mathbf{J}(\mathbf{r}')\| \mathrm{d}v'. \tag{2.9}$$

Thus, U is the solution of an exterior Neumann problem, with $\partial U/\partial n = 0$ on the surface of the sphere and $U \to$ constant as $r \to \infty$, and is thus unique up to an additive constant. Since $U =$ constant is the solution, the magnetic field is zero.

The magnetic field generated by currents in a spherically symmetric conductor can be calculated analytically. According to Sarvas (1987), the magnetic field is

$$\mathbf{B}(\mathbf{r}) = \frac{\mu_0}{4\pi} \int \frac{F\, \mathbf{J}_p(\mathbf{r}') \times \mathbf{r}' - \mathbf{J}_p(\mathbf{r}') \times \mathbf{r}' \cdot \mathbf{r}\, \Delta F}{F^2} \mathrm{d}v', \tag{2.10}$$

where

$$
\begin{aligned}
F &= \|\mathbf{a}\|(\|\mathbf{r}\|\,\|\mathbf{a}\| + \|\mathbf{r}\|^2 - \mathbf{r}' \cdot \mathbf{r}), \\
\Delta F &= (\|\mathbf{a}\|^2/\|\mathbf{r}\| + \mathbf{a} \cdot \mathbf{r}/\|\mathbf{a}\| + 2\|\mathbf{a}\| + 2\|\mathbf{r}\|)\mathbf{r} - (\|\mathbf{a}\| + 2\|\mathbf{r}\| + \mathbf{a} \cdot \mathbf{r}/\|\mathbf{a}\|)\mathbf{r}', \\
\mathbf{a} &= \mathbf{r} - \mathbf{r}'.
\end{aligned}
$$

When calculating the fields with a BEM, the inside surface of the skull is tessellated based on anatomical magnetic resonance images (Seppä, 1997; Lötjönen et al., 1999; Dale et al., 1999). Also the outside of the skull and scalp can be modeled, although the importance of these for MEG studies is smaller (Hämäläinen and Sarvas, 1989). The magnetic field with a piecewise homogeneous conductor can be calculated from the surface integral (Geselowitz, 1970)

$$\mathbf{B}(\mathbf{r}) = \mathbf{B}_0(\mathbf{r}) + \frac{\mu_0}{4\pi} \sum_{i,j} (\sigma_i - \sigma_j) \int_{S_{ij}} V(\mathbf{r}') \frac{(\mathbf{r} - \mathbf{r}')}{\|\mathbf{r} - \mathbf{r}'\|^3} \times \mathrm{d}\mathbf{S}', \tag{2.11}$$

where σ_i are the conductivities of the homogeneous compartments and S_{ij} their boundaries and $\mathbf{B}_0(\mathbf{r})$ is the field generated by the primary currents alone, Eq. (2.5). The potential on the surfaces can be calculated from the integral equation (Barnard et al., 1967; Geselowitz, 1967)

$$V(\mathbf{r}) = \frac{\sigma_0}{\sigma(\mathbf{r})} V_0(\mathbf{r}) - \frac{1}{4\pi} \sum_{i,j} \frac{(\sigma_i - \sigma_j)}{\sigma(\mathbf{r})} \int_{S_{ij}} V(\mathbf{r}') \frac{(\mathbf{r} - \mathbf{r}')}{\|\mathbf{r} - \mathbf{r}'\|^3} \times \mathrm{d}\mathbf{S}', \tag{2.12}$$

where σ_0 is the unit conductivity $1/(\Omega\mathrm{m})$ and V_0 is the potential generated by primary currents in unbounded medium with unit conductivity:

$$V_0(\mathbf{r}) = \frac{1}{4\pi\sigma_0} \int \frac{\nabla' \cdot \mathbf{J}_p}{\|\mathbf{r} - \mathbf{r}'\|} \mathrm{d}v' \tag{2.13}$$

When FDM or a FEM is used, the whole conducting volume is discretized. With FDM, the volume is filled with regularly spaced nodes with different conductances.

The conductances can be obtained by segmenting a MR image of the subject and using previously measured values for each tissue type. With FEM the volume is divided into elements, each of which are assumed to have a fixed conductance. With both methods, the potential within the whole volume is solved first, then the volume currents produced by those, and when the total current is known, the magnetic field can be calculated using Eq. (2.5).

Due to the principle of linear superposition, the sensitivity of an MEG sensor to different parts of the brain can be described using lead fields $\mathscr{L}(\mathbf{r})$ (Malmivuo, 1976; Tripp, 1983). Thus, the signal produced by a sensor is related to the source distribution as

$$b_i = \int \mathscr{L}_i(\mathbf{r}') \cdot \mathbf{J}_p(\mathbf{r}') \, \mathrm{d}v'. \tag{2.14}$$

The current distribution

$$\mathbf{J}_p(\mathbf{r}') = \delta(\mathbf{r}' - \mathbf{r}_d) \, \mathbf{q}_d, \tag{2.15}$$

where $\delta(\mathbf{r})$ is the Dirac function, is called a current dipole. It represents a point-like current at location $\mathbf{r}_d$ with fixed current orientation. The current parameter $\mathbf{q}_d$ is called the dipole moment. For a point-like sensor coil with location $\mathbf{r}$, orientation $\mathbf{n}$, and unit gain, the component of the lead with the orientation of dipole moment $\mathscr{L}(\mathbf{r}_d, \mathbf{q}_d)$ can be calculated as the component of the magnetic field in the sensor location $\mathbf{r}$ produced by an unit current dipole $(\mathbf{r}_d, \mathbf{q}_d)$ with $\|\mathbf{q}_d\| = 1$. Substituting Eq. (2.15) into Eq. (2.10) yields the lead field of the point-like sensor with the spherical conductor model:

$$\mathscr{L}(\mathbf{r}_d, \mathbf{q}_d) = \frac{\mu_0}{4\pi F^2} \left(F \, \mathbf{q}_d \times \mathbf{r}_d - \mathbf{q}_d \times \mathbf{r}_d \cdot \mathbf{r} \, \Delta F \right) \cdot \mathbf{n}. \tag{2.16}$$

Lead fields of realistic sensors coils (section 2.3) can be obtained by integrating Eq. (2.16) over the area constrained by the coils.

2.3 Measuring neuromagnetic fields

The magnetic fields produced by the brain are very weak. Typical magnetic field outside of the head evoked by external stimulation has an amplitude of 100 fT, which is on the order of 10^{-9} of the static geomagnetic field of the earth. Therefore, the measurement devices have to be extremely sensitive, and external magnetic noise must be attenuated.

Weak magnetic fields can be conveniently measured with a superconducting quantum interference device (SQUID) (Zimmerman et al., 1970) that consists of a superconducting loop intercepted with usually two thin, insulating layers, the Josephson (1962) junctions. When a suitable bias current is fed through the SQUID, the voltage across the SQUID varies periodically depending on the external magnetic field (Fig. 2.3). A voltage linearly proportional to the external magnetic field can be generated by keeping the SQUID at a constant magnetic field using a feedback coil and measuring the strength of the feedback.

The magnetic field is brought to the SQUID with a flux transformer consisting of a pickup coil and a signal coil. The shape of the pickup coil determines the spatial sensitivity pattern of the sensor. A simple loop, magnetometer, measures one component of the magnetic field. It is maximally sensitive on two locations on both sides of the source current (Fig. 2.4a). Since most of the external magnetic noise is generated much

Figure 2.3:   An example setup for measuring magnetic fields with a SQUID. *(a)* A flux transformer, consisting of a pickup and a signal coil, couples the SQUID with the external magnetic field. The electronics drive a bias current through the SQUID and amplify the signal. *(b)* The voltage over the SQUID has periods of $\Phi_0 = 2.07$ fWb. The feedback coil is used to linearize the output at the working point.

Figure 2.4:   Examples of pickup coils for detecting neuromagnetic responses: a magnetometer *(a)*, a first-order axial gradiometer *(b)*, and a first-order planar gradiometer *(c)*. Coils are shown at the locations where they measure the maximal signal from the magnetic field generated by a current dipole.

Figure 2.5: The sensor array of *Neuromag-122*™ neuromagnetometer *(a)*, comprising 61 elements each having two planar gradiometers, and the sensor array of *Neuromag Vectorview*™ *(b)*, comprising 102 elements each having two planar gradiometers and one magnetometer.

further away from the sensor than the interesting signals, the signal-to-noise ratio of the sensor can be increased by making the sensor more sensitive t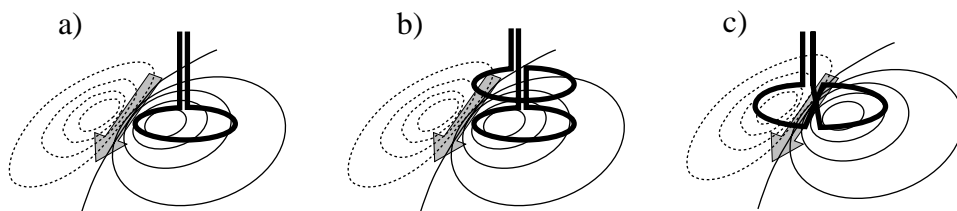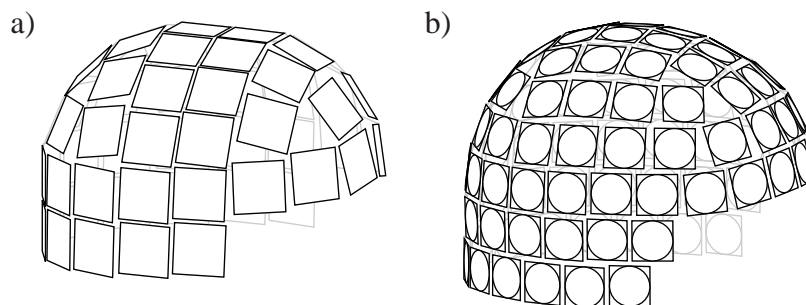o nearby sources. A first-order axial gradiometer achieves this with another coil on the top wound in the opposite direction (Fig. 2.4b). A first-order planar gradiometer has two opposite coils next to each other (Fig. 2.4c); this configuration is most sensitive to sources generated near and directly below the sensor.

To reduce the externally generated noise further, the measurements are usually performed in magnetically shielded rooms consisting of layers of aluminum and μ-metal. Low-frequency noise can be also attenuated with active compensation, in which current fed through external compensation coils is controlled to minimize the disturbance field measured inside the room.

The neuromagnetic measurements for the publications were done using *Neuromag-122*™ (Ahonen et al., 1993) and *Neuromag Vectorview*™. The *Neuromag-122*™ comprises 122 planar gradiometers (Fig. 2.5a). The sensors are arranged in 61 elements, each containing two planar gradiometers with orthogonal orientations. The device was placed in a magnetically shielded room with three aluminum and μ-metal layers. The *Neuromag Vectorview*™ has 102 elements, each containing two planar gradiometers and one magnetometer, having a total of 306 sensors (Fig. 2.5b). The device was placed in a magnetically shielded room with two aluminum and μ-metal layers and active noise compensation.

Modeling of the current sources of measured magnetic fields requires information on the position and orientation of the sensors in relation to the head. This is usually obtained by feeding currents through coils attached to the surface of the head (Knuutila et al., 1985; Erné et al., 1987; Ahlfors and Ilmoniemi, 1989; Incardona et al., 1992; Fuchs et al., 1995). The locations of the coils with respect to the sensor array are then computed on the basis of the measured signals.

2.4   Applications of magnetoencephalography

Although clinical applications are also emerging, magnetoencephalography has been mainly used for basic research. MEG, having high temporal specificity, lends itself readily to the study of sensory processing. Because of their relatively focal current dis-

tributions, the somatosensory (Brenner et al., 1978) and auditory systems (Hari et al., 1980) are very suitable for MEG studies. The visual system, being the primary sense of humans, has also been studied (Brenner et al., 1975). Outside the mainstream, also olfaction (Kettenmann et al., 1996) and pain (Hari et al., 1983) have been explored.

After magnetometer arrays covering the whole head had been introduced, an increasing number of studies of higher cognitive functions have been performed, for example, studies of visual perception of faces (Halgren et al., 2000), language-specific phonetic memory (Näätänen et al., 1997), and picture naming (Salmelin et al., 1994).

Most of the current MEG measurements study responses evoked by different stimuli. Due to the temporal resolution of MEG, the evoked response studies can determine which brain areas are activated and in which order. For example, in picture naming, first activated areas are the occipital visual areas, followed by frontal temporoparietal language areas, and finally the motor areas responsible for speech generation.

MEG has also been employed to study the spontaneous activity within the brain and its reactivity. The main emphasis has been in the rhythmic activity, such as 8–13 Hz α-rhythm generated near the parieto-occipital sulcus (Williamson et al., 1989) or the μ-rhythm generated in the sensorimotor areas of the brain (Tiihonen et al., 1989). Rhythmic brain activities driven with stimulation (Narici et al., 1998) or correlated with other electrophysiological signals (Salenius et al., 1997) have been studied as well.

The most important clinical applications of MEG have been localizing brain areas causing epileptic seizures (Barth et al., 1982; Paetau et al., 1990) and mapping of important brain areas before brain surgery (Gallen et al., 1993; Mäkelä et al., 2001). Along with the studies of the cognitive functions, possible physiological reasons for cognitive deficits such as dyslexia (Salmelin et al., 1996) and autism (Lewine et al., 1999) have been investigated.

The range of possible applications for modern MEG is very wide, which can be seen in the number different fields of neuroscience represented in the latest conferences on biomagnetism (Yoshimoto et al., 1999; Nenonen et al., 2001).

Chapter 3

Source modeling

3.1 Estimation

General estimation methods

Finding out the neuronal currents based on the MEG measurements is an estimation problem. When a suitable model for the activation of the source areas has been defined, the measured signals are used to specify the parameters of the model, typically telling the strength of current in different parts of the brain.

The mathematical basis of estimation methods were developed in the 18th and early 19th centuries (Sorenson, 1980). In 1763 an essay by Thomas Bayes was published describing the idea that the *a priori* probability distribution and a measurement provide the *a posteriori* distribution describing the knowledge about possible values of the parameter. In 1777, Daniel Bernoulli described the method of maximum likelihood stating that one should select the parameter value making the obtained values most probable. In the beginning of the 19th century Adrien-Marie Legendre and Carl Friedrich Gauss independently invented the method of least squares; Gauss used the normal distribution for describing the measurement errors and used that to give a sound theoretical basis for the method (Gauss, 1863).

The importance of the work by the 18th and 19th century mathematicians is seen also in this thesis, as most of the estimation methods used are based on the least-squares approach and on maximizing the *a posteriori* probability distribution. However, one field where the 20th century brought many new approaches was the study of stochastic processes. Andrey Kolmogorov and Norbert Wiener studied the parameter estimation from continuous measurements and Kalman (1960) published an efficient way of updating parameter estimates with new observations, which is presently known as the Kalman filter.

Many estimation problems in MEG are ill-posed, *i.e.*, several parameter combinations may produce the same results or large changes in the parameters may produce only small changes in the measured variables (section 3.2). Backus and Gilbert (1970) considered such linear problems in view of their resolution kernels and suggested an approach where the spatial sensitivity of the estimate is as close to the preferred one as possible. Another approach is to make the problem well-posed by use of regularization (section 3.5). Generally used regularization methods are singular value truncation that constrains the estimate to a well-behaving subspace and the Tikhonov regularization (Tikhonov and Arsenin, 1977) that explicitly favors smaller parameters. The estimates can also be regularized by assuming a suitable *a priori* distribution for the parameters of the model and calculating the *a posteriori* probability estimate Tarantola (1987).

Estimation methods for magnetoencephalography

The most common source model for MEG is the overdetermined dipole model (section 3.3). When successive samples are modeled with a single dipole (Brenner et al., 1978; Tuomisto et al., 1983), the location of the dipoles may change over time leading to a moving dipole. Moving dipole models have been widely used for magnetic fields generated in the heart (Nenonen, 1994). In the brain, however, the same population of neurons is likely to be active over a time period. Therefore, the neuromagnetic dipole models include the assumption that the location and orientation are fixed, but the amplitude may vary as a function of time (Scherg, 1990; Mosher et al., 1992). Multiple, spatially separated sources can be modeled by several fixed dipoles.

The multiple signal classification (MUSIC) method (Schmidt, 1986; Mosher et al., 1992; Sekihara et al., 1997; Mosher and Leahy, 1998) can be also used to create a multidipole model. The method divides the data, represented by its spatial autocorrelation matrix, into orthogonal signal and noise subspaces based on the strength of the signals. To find the locations of multiple sources, the field generated by a single dipole is calculated and locations where most of the calculated field falls into the signal subspace are considered plausible source locations. The MUSIC method additionally assumes that the amplitude time series of the different sources are not linearly dependent.

Distributed estimates (section 3.5) for MEG were first applied by Hämäläinen and Ilmoniemi (1984, 1994). Their minimum-norm estimate (MNE) selects the solution where the ℓ^2-norm of the current distribution was smallest. Since the plain MNE is still very sensitive to noise, they regularized it using singular value truncation. The source strengths were assumed *a priori* independent and having equal variances.

Several modifications of this approach have been proposed. For example, Dale and Sereno (1993) suggested constraining the source space into anatomically known locations and orientations and weighting the estimate based on *a priori* information. Pascual-Marqui et al. (1994) proposed an approach where the source strengths between the neighboring source locations are correlated.

Activity in nearby neurons is often connected. Although local connections with 1 mm distance and also longer horizontal connections up to 6–8 mm are common (Gilbert et al., 1996), the neurons with more than 1 cm distance can be on quite different functional areas that are not necessarily correlated. The MNEs tend to be unrealistically smooth even without the explicit assumption of spatial smoothness. An *ad hoc* method for obtaining focal estimates is to use weighted, iterated MNEs, where the areas where the estimated source strength is large have smaller costs (Ioannides et al., 1990; Dale and Sereno, 1993; Gorodnitsky et al., 1995). Focal estimates can be also be obtained with the minimum ℓ^1-norm estimates (Matsuura and Okabe, 1995; Fuchs et al., 1999), which can be justified also in the Bayesian framework (section 3.6).

When a brain area is known to be active, the activity as a function of time can be estimated also without explicitly modeling the other sources. This beamformer approach uses spatial filters that are designed to be most sensitive to signals generated in the region of interest (Robinson, 1989; Gross and Ioannides, 1999; Sekihara et al., 2001). This approach has also been applied to localization of brain areas with correlated activity (Gross et al., 2001).

Besides calculating a single estimate of the data, it is also possible to study the whole *a posteriori* distribution of the parameters (Gelman et al., 1995). The conclusions can be drawn, for example, by calculating marginal distributions of different parameters. The application of Bayesian data analysis to MEG source modeling (Schmidt

et al., 1999) is currently computationally rather demanding but has the flexibility for combination of different kinds of *a priori* information.

3.2 Problems and possibilities

Non-uniqueness

Different current distributions within the brain may yield exactly the same electromagnetic field outside the head (Helmholtz, 1853). Therefore, even with perfect measurements of the magnetic field, it would be impossible to know the current distribution uniquely.

Besides this theoretical non-uniqueness, the practical limits of the measurements complicate the modeling. Modern magnetometer arrays measure typically 100–306 samples of the magnetic field. However, since the lead fields of the sensors are correlated, the signals from whole sensor array are comparable to 50–100 uncorrelated measurements. Since the number of different brain areas and uncorrelated processes is much higher, it is impossible to estimate the currents for all activated brain areas without further assumptions.

To circumvent the non-uniqueness, some *a priori* information has to be added. Typical assumptions are that only few distinct brain areas are active at the same time, that the strength of the current in each location is relatively small, that the same areas are active over long periods of time, or that the sources are at locations known in advance based on the anatomy of the brain.

Without modeling, the resolution of MEG is several centimeters. For example, for a source in a known depth, the full-width half maximum of the lead field of a gradiometer can vary from 25 mm to 100 mm, depending on the depth and orientation of the source. On the other hand, when the source distribution can be modeled, the accuracy may be a couple of millimeters.

The success of modeling depends strongly on the simplicity of the model. For example, when it is known in advance that only a single, small brain area is activated, the current distribution can be modeled with a current dipole, and the accuracy for the estimating the center of the activated area can be close to 1 mm. But to distinguish the magnetic field produced by the single source from that produced by two simultaneous cortical sources, the separation of two parallel dipoles has to be roughly 3 cm (Hari et al., 1988; Lütkenhöner, 1998).

Noise

All MEG measurements are noisy. Within the interesting frequency range, the SQUID-based detectors and read-out electronics produce spatially and temporally rather uncorrelated noise. The magnetic noise from generators outside the magnetically shielded room is spatially correlated; the homogeneous components of the magnetic field are typically the noisiest ones. Temporally the noise consists mainly of low frequencies and signals produced by electrical devices, typically very close to 50 or 60 Hz and their harmonic frequencies. The subject being measured produces many magnetic artifacts; the sources include heart, eye and muscle movements, and possible magnetic material attached to the slightly moving subject. These produce mostly low-frequency spatially correlated noise.

Most of the MEG studies are targeted to certain subprocesses of the total brain activity. For example, evoked responses are often studied using the averaging paradigm, where only the brain activity that is temporally correlated with the stimulus presentation is considered interesting. In these cases the background brain activity is essentially noise that interferes with the measured signals.

The effect of the noise can be diminished by taking into account its statistical properties. The signal can be spatially, temporally, or spatio-temporally (Beucker and Schlitt, 1997) whitened, which may significantly improve the accuracy of estimation.

Since the estimation of the correlations needed for prewhitening may be difficult or computationally costly, some simplifications are often used. Temporally, if signal-to-noise ratio is assumed constant in a certain frequency range and zero elsewhere, the effect of whitening can be achieved by band-pass filtering to the correct frequency range. Spatially, if the signal-to-noise ratio is assumed constant in certain signal subspaces and zero elsewhere, the effect of whitening can be achieved by signal-space projection (SSP) (Uusitalo and Ilmoniemi, 1997).

The use of low-pass or possibly also high-pass filtering is standard practice in most of the MEG experiments. The SSP is applied in analysis of data recorded by the magnetometers of *Neuromag Vectorview*™ by removing the signal subspaces that are strongest in signals measured from an empty room. The noise subspaces can also be found for example by finding signals correlated with a known noise source such as the heart (Jousmäki and Hari, 1996) or by removing signals with non-typical higher order statistics using independent component analysis (Vigário et al., 2000).

The spatial correlation matrix of the background brain activity is roughly similar to that produced by dipolar sources with varying, uncorrelated amplitudes (de Munck et al., 1992). The background activity can be of the same level as the other noise sources combined, and it is especially difficult to remove since the interesting signals usually have similar spatial and temporal properties.

3.3 Conventional dipole modeling

When the extent of a source areas is small compared with the distance to the sensors, and when the orientations of the currents are roughly parallel, the measured magnetic field resembles that generated by a current dipole. When n_d areas producing dipolar fields are active, the magnetic fields measured with n_c sensors at n_t time instants can be written in matrix form

$$\mathbf{B} = \mathbf{G}(\mathbf{r}, \mathbf{q})\,\mathbf{Q} + \mathbf{N}, \tag{3.1}$$

where the $n_c \times n_t$ matrix $\mathbf{B}$ is the measured signal, the $n_c \times n_d$ $\mathbf{G}(\mathbf{r}, \mathbf{q})$ comprises the signals generated by unit dipoles with given locations $\mathbf{r} = (x_1, y_1, z_1, \ldots, x_{n_d}, y_{n_d}, y_{n_d})$ and orientations $\mathbf{q} = (q_{1x}, q_{1y}, q_{1z}, \ldots, q_{n_dx}, q_{n_dy}, q_{n_dz})$ in its columns, the $n_d \times n_t$ matrix $\mathbf{Q}$ comprises the strength of the sources as a function of time on its rows, and the $n_c \times n_t$ matrix $\mathbf{N}$ describes the noise.

When the noise is Gaussian and white, the maximum likelihood estimate of the dipole parameters $(\mathbf{r}, \mathbf{q})$ can be calculated by minimizing the least-squares cost function

$$E(\mathbf{r}, \mathbf{q}, \mathbf{Q}) = \|\mathbf{B} - \mathbf{G}(\mathbf{r}, \mathbf{q})\,\mathbf{Q}\|_F^2, \tag{3.2}$$

where the square of the Frobenius norm, $\| \cdot \|_F^2$, is the sum of the squares of the elements of the matrix.
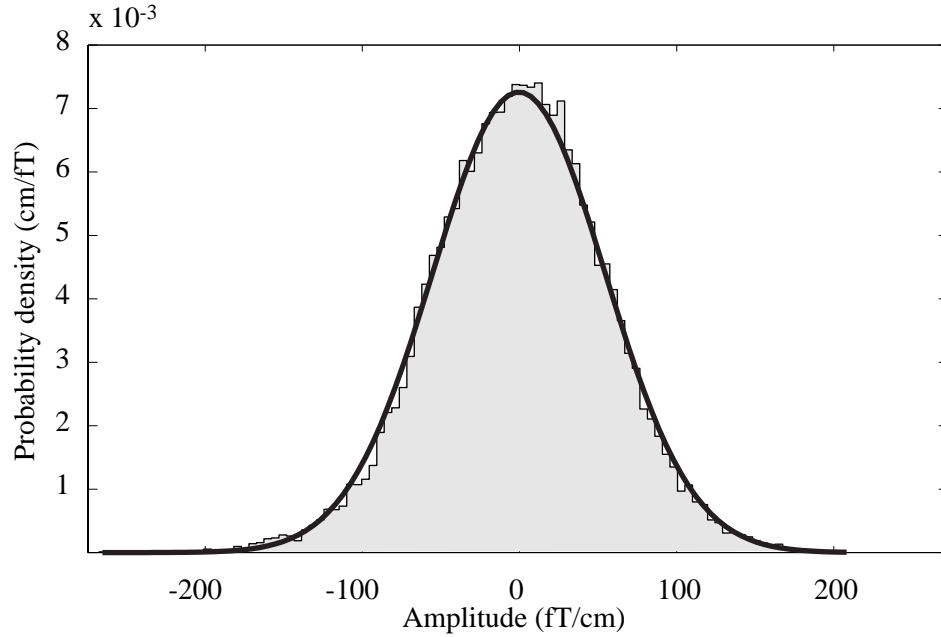
Figure 3.1:   Amplitude distribution of the neuromagnetic signals measured while a subject was resting in a magnetically shielded room: signal from a planar gradiometer (*gray histogram)* and fitted normal distribution (*solid line).*

Taking into account the spatial correlation of the noise, $\mathbf{C}_n$, yields the weighted least-squares cost function

$$E_w(\mathbf{r}, \mathbf{q}, \mathbf{Q}) = \| \mathbf{C}_n^{-1/2} (\mathbf{B} - \mathbf{G}(\mathbf{r}, \mathbf{q}) \, \mathbf{Q}) \|_F^2. \tag{3.3}$$

Although the oscillatory background activity and some external artifacts may have a very non-Gaussian distribution, each sensor is sensitive to several noise sources, which usually makes the distribution rather close to the normal distribution (Fig. 3.1). Especially when the averaging paradigm is applied the requirement of Gaussianity can be rather safely assumed to hold.

The true source areas in the brain are not point-like, but it is supposed that roughly an 1 cm^2 or bigger area produces the clearly detectable signals (Hämäläinen et al., 1993). Therefore, the calculated field pattern of the dipole does not exactly match the true source and the residual field will slightly interfere with the estimation of other sources. However, from the typical measuring distances, the difference is too small to be even detected from ordinary MEG measurements (Tarkiainen, 1997; Nolte and Curio, 1999). A more significant source of errors has been the conductor model used in the forward calculations. According to Buchner et al. (1995), the difference between dipole locations estimated with a spherical model and a BEM varies from 2 mm for superficial sources to at least 7 mm for deep sources.

The multidipole models need to have a specified number of sources. The number can be selected manually or by different mathematical criteria, but in any case the number of areas really involved in brain processes being studied is generally larger than the number of sources that can be detected and localized. The sources that are not modeled can be viewed as sources of correlated noise in the measurements.
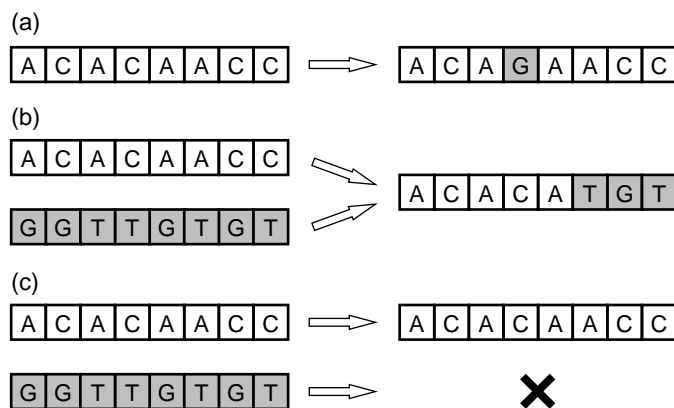
Figure 3.2:   The basic operations of genetic algorithms are mutation (*a*), cross-over (*b*), and selection (*c*).

3.4   Global optimization in dipole modeling (P1)

If a single brain area resembling a current dipole is activated, dipole modeling is straightforward. An initial estimate of the dipole location can be generated either based on the maximal measured gradient when planar gradiometers are used or from the locations of the field extrema when magnetometers or axial gradiometers are used. The cost function (3.2) has only three non-linear parameters and is rather well-behaved.

However, if several sources are activated during the same time period, there is no simple way of generating initial estimates and the cost function has more parameters and many local minima making the optimization highly dependent on the initial guess. Publication P1 discusses methods for solving this problem efficiently and reliably.

To speed up the calculation, the cost function Eq. (3.2) was simplified by having only the non-linear location $\mathbf{r}$ as a parameter; the optimal fixed orientation was calculated for each source location.

During the optimization there may be cases where a potential source configuration has dipoles very near to each other. In these cases calculating the value of the cost function becomes ill-conditioned, and numerical instability may hinder the computations. Therefore Tikhonov regularization (Tikhonov and Arsenin, 1977) was applied by adding the squared sum of the source amplitudes to Eq. (3.2).

Several algorithms aimed to find the smallest minima of cost function have been developed (Törn and Zhilinskas, 1989). These global optimization algorithms use different criteria to concentrate the search on the areas where the global minimum is most likely found, thus decreasing the number of cost function evaluations needed. In publication P1 three different approaches were adapted to the specific problem of solving the multidipole model cost function: a clustering method using conventional local optimization with random starting points and concentrating on the areas where the local algorithms concentrate, simulated annealing (Kirkpatrick et al., 1983) applying the Metropolis simulation (Metropolis et al., 1953) to function minimization, and a genetic algorithm (Holland, 1975) emulating the evolution of species. The genetic algorithm with suitable parameters proved to give the correct solution most reliably with a constrained number of cost function evaluations.

The applied genetic algorithm describes each set of location parameters $\mathbf{r}$ as a binary sequence called a chromosome. The chromosomes are mutated, new offspring

are produced by combining parts of existing chromosomes, and the chromosomes producing largest errors are discarded (Fig. 3.2).

The chromosomes were selected and combined by selecting randomly groups of four chromosomes, discarding the two worst ones and creating new ones by selecting each dipole coordinate with equal probability from the two best chromosomes. The values were mutated by randomly changing one bit of the binary representation or by adding a normally distributed random value; the impairing mutations were rejected with a probability depending on the increase of the cost function. The variance of the random value was adaptive and the probability scale of rejections was slowly decreased (Corona et al., 1987). To speed up the convergence of the algorithm, the total number of chromosomes was decreased by clustering the chromosomes with a c-means algorithm (Schalkoff, 1992) and by selecting a representative chromosome for each cluster.

The algorithm was evaluated using simulated MEG measurements with 2 or 4 sources. With the parameters described in publication P1, the algorithm was capable of finding the correct source configuration with a sufficient accuracy in all trials without extensive computational demands. Calculating the estimate with a typical workstation of 1995 took 1–5 min; with a modern workstation the same task takes 15 s–1 min.

When a few more sources were estimated, the genetic algorithm still performed well if the total number of different chromosomes was increased proportionally. However, when a very large number of sources were estimated using one time period, the number of source combinations explaining almost all the measured data soared and the results were not very robust.

Also, with several simultaneous sources, the unrealistic assumptions of the models hamper the estimation. Correlated noise and sources that are not modeled may produce dipolar-looking ghost sources. By selecting time intervals and model orders appropriately, the multidipole estimation may produce reasonable results, as demonstrated by the naming task data in publication P1. However, some prior information or scientific expertise is usually needed for modeling complex data.

Different global optimization methods for MEG or EEG source estimation have been proposed also by other groups. A multi-start method, essentially similar to the clustering method but without the clustering phase, has been applied by Huang et al. (1998) and simulated annealing by Gerson et al. (1994) and Haneishi et al. (1994). Publication P1 aimed mainly at finding one reasonable optimization algorithm and not comparing the different methods. Although the applied genetic algorithm was the most efficient in the comparisons, also the other methods can be used with suitable parameters and sufficient calculation time. They also may have some other desirable properties. For example, the clustering method is good at finding several local minima, which can be useful for comparing different plausible solutions.

The MUSIC approach is in some ways similar to using the automated least-squares multidipole modeling: the models assume several dipolar sources, and since the MUSIC algorithms typically scans through the whole source space, no initial guesses are needed. In MUSIC the number of sources (dimensions of the signal space) affects less the locations of estimated sources. On the other hand, the least-squares estimation can tolerate temporally correlated sources better.

3.5 Distributed current estimates

The dipole model is an example of an over-determined parametric model, where the degrees of freedom of the measured data exceed the number of parameters being estimated. However, when more flexible models with many parameters are needed, underdetermined models must be used.

The dipole model, Eq. (3.1), can be extended so that the dipole locations and orientations are predefined and cover the volume where sources can be found with a sufficient accuracy. Typically the number of sources, n_d, then exceeds the number of sensors, n_c. If a single time point is considered, the measured field vector $\mathbf{b}$ can be modeled as

$$\mathbf{b} = \mathbf{G}\,\mathbf{q} + \mathbf{n}, \tag{3.4}$$

where the $n_c \times n_d$ matrix $\mathbf{G}$ is a discretized version of the lead fields Eq. (2.14) and includes the fields produced by unit dipoles in different source locations. The n_d-dimensional vector $\mathbf{q}$ includes the discretized source amplitudes at different locations and orientations, and $\mathbf{n}$ is the noise.

If the noise and source strengths are *a priori* normally distributed with zero means and correlation matrices $\mathbf{C}_n$ and $\mathbf{C}_q$, the maximum *a posteriori* probability estimate minimizes the weighted least-squares error function (Tarantola, 1987)

$$E(\mathbf{q}) = (\mathbf{b} - \mathbf{G}\,\mathbf{q})^t\,\mathbf{C}_n^{-1}\,(\mathbf{b} - \mathbf{G}\,\mathbf{q}) + \mathbf{q}^t\,\mathbf{C}_q^{-1}\,\mathbf{q}. \tag{3.5}$$

The first term of the equation is actually the same as in the weighted estimate for parametric models, Eq. (3.3). However, minimizing that when $n_d > n_c$ would not yield an unique solution. The second term $(\mathbf{q}^t\,\mathbf{C}_q^{-1}\,\mathbf{q})$ makes, with a suitable $\mathbf{C}_q$, the minimum unique by preferring solutions with small total currents. This method for obtaining an estimate for under-determined system is also known as Tikhonov regularization (Tikhonov and Arsenin, 1977). If the noise is assumed white, standard deviation of the amplitude being σ_b, and source strengths spatially uncorrelated with standard deviation being σ_q, the cost function reduces to

$$E(\mathbf{q}) = \sigma_b^{-2}\,\|\mathbf{b} - \mathbf{G}\,\mathbf{q}\|_2^2 + \sigma_q^{-2}\,\|\mathbf{q}\|_2^2, \tag{3.6}$$

where $\|\cdot\|_2$ is the Euclidean or ℓ^2-norm.

In the MNE regularized using singular value truncation (Hämäläinen and Ilmoniemi, 1994), instead of using the whole gain matrix $\mathbf{G}$, a subspace consisting of only the largest singular vectors is used. When the dimension of the subspace is smaller than the number of measurements, this approach yields a unique solution. The estimate can be computationally efficiently calculated as

$$\widehat{\mathbf{q}} = \mathbf{G}^t\,(\mathbf{G}\,\mathbf{G}^t)^*\,\mathbf{b} \tag{3.7}$$

where $(\cdot)^*$ denotes the regularized inverse that ignores the subspaces with small values. The result is concordant with Eq. (3.5) when the matrix $\mathbf{C}_n$ has very large values in the non-selected subspaces.

For other imaging modalities, especially fMRI and PET, statistical parameter maps (SPMs) have been widely used to assess the significance of the estimated effects (Friston et al., 1995). The idea is to consider each location in the estimate independently, and calculate the probability of getting the results by chance using a null hypothesis that all the estimated activation in the specified location comes from noise. Using

conventional levels of statistical significance, several locations may seem active even under the null hypothesis due to multiple comparisons, but this can be taken into account in the statistical reference by selecting higher thresholds or by considering the number of areas above threshold. Corrected levels depend on the size of the image and spatial autocorrelation of the noise.

SPMs have been also used in connection of MEG data (Dale et al., 2000). However, since the MNE in certain location is also sensitive to activation in other locations, the MEG SPM has to be interpreted appropriately. The null hypothesis for MEG SPM is that there is no activation in any brain area the MNE is sensitive to. Strictly speaking that would mean that MEG SPM can answer the question whether there is activity anywhere in the brain, but not whether there is activity in a certain brain area. Of course MEG SPM can also be thought of as a refined imaging method, but the significance values obtained do not consider the uncertainty of the localization. For example, if the statistical significance of an estimate in a specified area is high, the likelihood of having the true activation at that brain area may still be low. Also, the size and shape of the area of the estimate above the threshold are more related to the signal-to-noise ratio of the measurement than to the true extent of the source area.

Considering the limitations, MEG SPM provides a framework to handle the problem of multiple comparisons in MEG analysis. In many cases, the multiple comparisons are implicit because of the subjectivity in data analysis. With dipole modeling, for example, a time and subset of the sensors that are compatible with a dipole model are often selected based on the measured data itself. Thus the explanation of the used model is one of the best of all the combinations of different times and weighting functions used. The MNE makes this more explicit by always producing estimates for several brain areas and times. Thus it is more straightforward to get an appropriate correction for the significance of the total activation. The methods used for fMRI and PET SPM can be applied also to MEG, taking into account the spatiotemporal correlations in the estimate, although some assumptions, such as spatial stationarity of the noise, may not hold very well.

3.6   Minimum current estimate (P2)

Even though the true source would be generated in a small patch of cortex, the minimum-norm estimate assuming *a priori* normally distributed source strengths yields estimates where the sources tend to be non-physiologically smooth and wide-spread. One reason is that the normal *a priori* distribution can be an unrealistic assumption. When distinct, focal source areas are activated, the kurtosis of the distribution of current amplitude is also bigger, *i.e.*, very strong and very weak currents are more likely than the normal distribution would suggest.

The assumption of focal estimates can be taken into account by modifying the *a priori* distribution of the source strengths, which in turn affects the latter term in cost function (3.6). For example, if source strengths are assumed exponentially distributed (Fig. 3.3) with standard deviation σ_q, measurement $\mathbf{b}$ yields the *a posteriori* probability density function

$$\begin{aligned} f(\mathbf{q}\,|\,\mathbf{b}) &= f(\mathbf{b}\,|\,\mathbf{q})\,f(\mathbf{q})/f(\mathbf{b}) \\ &= e^{-\sigma_b^{-2}\|\mathbf{b}-\mathbf{G}\,\mathbf{q}\|_2^2}\,e^{-\sigma_q^{-1}\|\mathbf{q}\|_1}\,c, \end{aligned} \qquad (3.8)$$

where where the ℓ^1-norm $\|\cdot\|_1$ is the sum of absolute values of the vector components
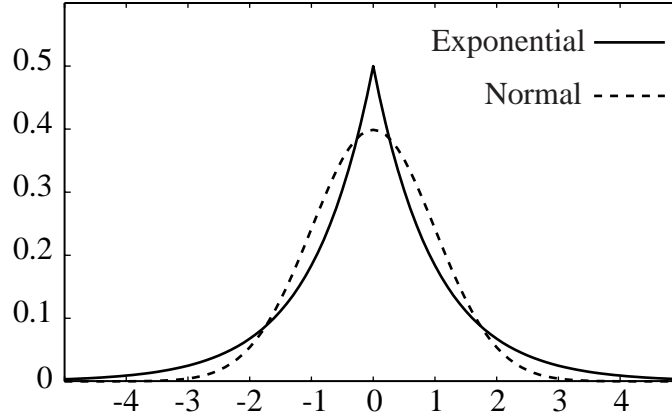
Figure 3.3:   The exponential *a priori* distribution of source strength (*solid line*) pro-
duces more focal estimates than the normal distribution (*dashed line*).

and *c* is normalizing constant. The maximum *a posteriori* probability estimate is thus
the current distribution **q** minimizing the cost function

$$E(\mathbf{q}) = \sigma_b^{-2} \|\mathbf{b} - \mathbf{G}\,\mathbf{q}\|_2^2 + \sigma_q^{-1} \|\mathbf{q}\|_1, \tag{3.9}$$

The publication P2 describes an MEG modeling method based on this approach: the
minimum current estimate (MCE).

Using different ℓ^p-norms in the field and current cost of function (3.6) modifies
the spread and robustness of the estimate (Tarantola, 1987). Using norms with small
p for the field cost yields estimates that are more tolerant to outliers in the data. The
ℓ^1-norm for over-determined systems was developed by R. J. Boscowich already in the
18th century and used later by P.-S. Laplace (Gauss, 1863), cited in Tarantola (1987).
Using norms with small *p* for the current cost yields more focal estimates. Minimizing
the ℓ^1-norm gives almost surely maximally sparse estimates: minimizing it with certain
number of constraints yields a result with the number of non-zero elements less or
equal to the number of constraints. Also estimates with norms $p < 1$ (Leahy et al.,
1988; Beucker and Schlitt, 1996) have been proposed.

Implementations of the minimum ℓ^1-norm estimate for MEG with different reg-
ularization assumptions have been independently developed. Matsuura and Okabe
(1995, 1997) use ℓ^∞-norm as field cost in Eq. (3.9), which is compatible with uni-
formly distributed noise in the measurements; Fuchs et al. (1999) use ℓ^1-norm as field
cost in Eq. (3.9), which is compatible with exponentially distributed noise in the mea-
surements. Since the measurement noise is rather normally distributed, the incorrect
norms used for the field cost increase the effect of noise in the estimates.

The typical number of possible source locations in a discretized MNE exceeds
1000. Minimizing a general function with so many free parameters tends to be either
inaccurate or extremely time-consuming. However, some specific models allow com-
putationally feasible estimates. The solution of the minimum ℓ^2-norm estimate can be
calculated using pseudo-inverse, and is thus computationally efficient. For more focal
estimates, the minimum ℓ^1-norm estimate with slight modifications can be efficiently
calculated using linear optimization.

The current cost in function (3.9) is already linear, but the field term is not. If the
weight of the field part is very high, corresponding to relatively small noise level σ_b,

minimization of the whole function can be replaced with the constrained minimization of the current term:

$$\min \|\mathbf{q}\|_1 \text{ subject to}$$
$$\mathbf{G}\,\mathbf{q} = \mathbf{B} \tag{3.10}$$
$$\mathbf{q} \geq 0.$$

In MCE, this estimate was regularized by applying singular value truncation to the constraints. This has the additional benefit that the number of constraints for the problem (3.10) decreases, thus decreasing the computational demands. The linear optimization problem was solved using revised simplex method which decreases the computation time substantially when the number of constraints is small compared to the number of parameters (Orchard-Hays, 1968). The implementation was based on the LP-solve library by Michel Berkelaar and Jeroen Dirks (Berkelaar, 2001).
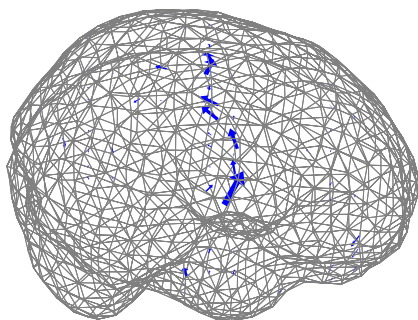
The formulation of function (3.10) assumes that the orientations of the currents are fixed in advance. Several sources with different orientations can be placed at the same location and their combinations can span all the orientations, but the predefined orientations will be preferred, since the ℓ^1-norm of two components will be larger than their ℓ^2-norm. In MCE a minimum ℓ^2-norm estimate of the same data is calculated first and its current orientations are applied also for the ℓ^1-norm. The MEG detector arrays used in the study, *Neuromag-122*™ and *Neuromag Vectorview*™, have gradiometer pairs that give the orientation information more directly than magnetometers, and thus the orientations of the sources can usually be obtained accurately also using different source models.

Visualization of the 3-dimensional current distribution of MCE has a trade-off between showing the complete information and relating the information to the underlying anatomy. The complete current distribution can be presented, for example, as a set of 3-dimensional arrows (Fig. 3.4a), but activity from different parts of the brain will be overlaid and perceiving the true locations is difficult without rotating the arrow set. Another method is to project all the activity to the surface of the brain (Fig. 3.4b); thus images from a few angles will present all the activation. The depth of the sources and orientation of the currents are difficult to visualize using this approach, but this method provides a good overview also with static images. To show the exact anatomical location of the estimated activated areas, slices of an anatomical background image can be overlaid with a color-coded estimate (Fig. 3.4c).
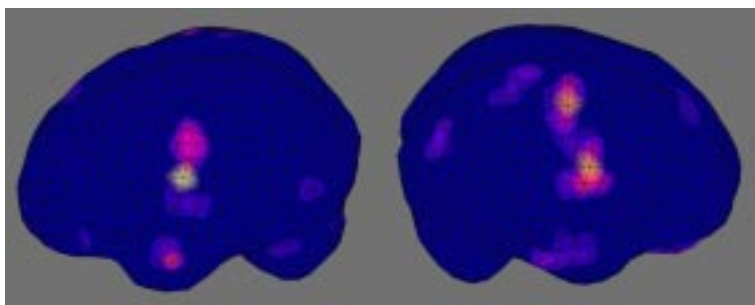
The temporal information adds a fourth dimension to the estimate. An illustrative, qualitative way to visualize that is to use any of the visualization methods and combine consecutive images into a movie. A more quantitative way is to select a region of interest (ROI) and plot the activity integrated over this region. This approach has been widely used to see the activity of, for example, fMRI data. The MCE results have two differences compared to fMRI. First, the spatial inaccuracy of the estimate should be reflected also in the visualization of the amplitude. Second, the orientation of the current provides very useful additional information helping differentiate close-by sources. To compensate for spatial inaccuracy, the ROIs used in studies P5–P7 were extended so that the activity close or beyond the surface of the ROI were added with smaller weights than activity in the center. The orientation information was used by projecting the sources with different orientations to a selected orientation before calculating the average.

When making statistical inference based on MCE results, the uncertainty of the location and the non-Gaussian distribution of the estimate should be taken into account. Smoothing the estimate temporally and spatially increases the tolerance to spatial er-

a)

b)

c)

Figure 3.4:   Visualization of MCE results *(a)* as 3-dimensional arrows, *(b)* projected to the brain surface, and *(c)* as an overlay on a slice of an anatomical image (Seppä and Hämäläinen, 2000)

rors and makes the distribution of the noise more Gaussian. Robust tests of differences between responses can be done by selecting the average activity within a time window in a region of interest and making a non-parametric test over results of different subjects. The anatomical differences between the groups can be taken into account by aligning the ROIs using piecewise linear (Talairach and Tournoux, 1988) or non-linear (Schormann et al., 1996) transformations of the anatomic brain images.

3.7   Head movement correction (P3)

In a typical neuromagnetic recording, several successive responses are averaged. The head is assumed to be still during the whole sequence. If the head has moved or if data from different measurement sessions are combined, the mixture of different head positions adds a location bias.

Subjects are typically asked to keep their head still during the measurements. This may be difficult even for cooperative subjects if the measurement is long or if the subject's task involves motor tasks. Therefore, the movement should either be eliminated or taken into account in the analysis. Using individual bite-bars helps avoiding head movements (Singh et al., 1997), but that makes the experiment uncomfortable for some subjects and can not be applied in experiments requiring verbal responses. Publication P3 studies the feasibility of measuring the head position during the whole measurement period and using this information to correct the estimates.

Measurement of head movements

The head position can be measured using coils attached to the head also during the measurement (de Munck et al., 2001). Two conditions have to be met: First, the dynamic range of the MEG measurement must be sufficiently large to enable the measurement of the brain signals together with the considerably stronger head position signals. Second, the head position signals must be separated from the brain signals.

In publication P3 the amplitude of the head position signals used was of the order of 10 000 fT/cm, which is 100 times stronger than typical brain signals. Thus, the dynamic range of the *Neuromag Vectorview*™ detector array with 16 bit resolution was sufficient. To make the removal of the head position signals easier, sinusoidal signals with frequencies above the frequencies of the brain signals were used (160, 162, 164, and 166 Hz). The signals were separated first by subtraction of signals with the known frequencies in 2 s time windows. Due to amplitude modulation caused by the head movements, this approach alone could not completely eliminate the head position signals. The rest was removed using a finite impulse response (FIR) low-pass filter. Using the FIR filter alone would have left significant startup and ending transients of the head position signals, but the combination of removing fixed amplitude signals and FIR filter produced clean brain signals.

To estimate the head position and orientation, first the signals produced by different coils on different sensors have to be extracted. In publication P3, the extracted constant amplitude during the 2 s window was used. This works very accurately if the head has not moved very much during the time period. However, the periods with larger head movements caused errors at this stage. In this work, these epochs were rejected from later analysis. If muscle and other artifacts caused by the movement are not a problem, the amplitude accuracy can be increased by decreasing the time window. In this

approach, the time window has still to be longer than the inverse of the frequency difference of different coils to keep the signals of different coils uncorrelated, so hardware allowing higher sampling and head position signal frequencies would be needed.

Shorter time windows of coil signals can also be used if they are modeled as a dynamic system. When a time window with n_w samples is considered one measurement, it can be related to the previous time window using the model

$$
\begin{aligned}
\mathbf{y}_{i+1} &= \mathbf{x}_{i+1} + \mathbf{n}_{i+1} \\
\mathbf{x}_{i+1} &= \sum_{j=1}^{n_c} a_{j,i+1} \mathbf{s}_{i+1} \\
a_{j,i+1} &= a_{j,i} + \Delta a,
\end{aligned}
\tag{3.11}
$$

where vectors $\mathbf{y}_i$, $\mathbf{x}_i$, and $\mathbf{n}_i$ are the measured and true coil signals and normally distributed noise during time window i, n_c is the number of coils, $a_{j,i}$ is the signal amplitude caused by coil j at time window i, $\mathbf{s}_{j,i}$ is the vector of the signals fed to coil j during time window i, and the change of the amplitude, Δa, is normally distributed. The amplitude parameters $a_{j,i}$ for this type of model can be efficiently estimated using extended Kalman filters (Kalman, 1960; Jazwinski, 1970).

The position and orientation of the head can be estimated from signal amplitudes by fitting the signals produced by the coils in different locations and orientations to the measured signal amplitudes. In publication P3 coils were modeled as magnetic dipoles.

Instead of first localizing the coils and then fitting the head position and orientation to the estimated coil locations, the head position and orientation were fitted directly: for each head position, the coil locations measured before the measurement were transformed to new locations, magnetic fields produced by magnetic dipoles with three orthogonal orientations in the given coordinates were calculated, and these patterns were used to model the measured amplitudes.

Both models for finding the head position have 12 linear parameters, the dipole moments. But while the free positions of the four coils would have 12 non-linear parameters, the head position and orientation comprise only 6 non-linear parameters. The smaller number of free non-linear parameters in the model makes finding the least-squares solution faster and more robust. The rotation of the head can be conveniently parametrized using quaternions (Hamilton, 1847).

The head position and orientation parameters $\mathbf{t}_i$ can be computationally estimated with an extended Kalman filter. When the estimates of the coil amplitudes during time window i are combined to vector $\mathbf{a}_i$, they can be modeled as

$$
\begin{aligned}
\mathbf{a}_{i+1} &= \mathbf{x}_{i+1} + \mathbf{n}_{i+1} \\
\mathbf{x}_{i+1} &= \mathbf{G}\left(\mathbf{r}_{i+1}\right) \mathbf{q}_{i+1} \\
\mathbf{r}_{i+1} &= \mathbf{T}(\mathbf{p}_{i+1}) \, \mathbf{r}_0 \\
\mathbf{p}_{i+1} &= \mathbf{p}_i + \Delta \mathbf{p}, \\
\mathbf{q}_{i+1} &= \mathbf{q}_i + \Delta \mathbf{q},
\end{aligned}
\tag{3.12}
$$

where $\mathbf{x}_i$ is the vector of true coil amplitudes during time window i, $\mathbf{G}(\mathbf{r})$ comprises the magnetic fields produced by three orthogonal magnetic dipoles in locations $\mathbf{r}$, $\mathbf{q}_i$ are the dipole moments, $\mathbf{r}_i$ are the locations of the coils, calculated from the original locations $\mathbf{r}_0$ using the linear transformation $\mathbf{T}$ related to the head position and orientation
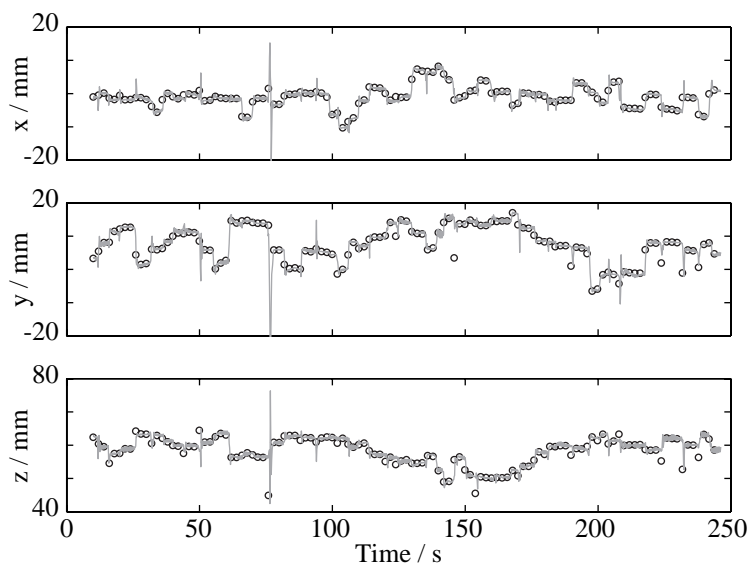
Figure 3.5: Head positions estimated from measured signals by considering each 2 s time window separately (circles) and by using Kalman filter with 167 ms time windows (lines).

parameters $\mathbf{p}_i$. The change of these parameters $\Delta\mathbf{p}$ the change of the dipole moments $\Delta\mathbf{q}$, and the estimation error of amplitude parameters noise $\mathbf{n}_i$ are normally distributed random variables.

Combining Eq. (3.11) and Eq. (3.12) allows computationally efficient estimation of the head position parameters. At each step, n_w samples are first measured and used to update the coil signal amplitude parameters $a_{j,i}$ of Eq. (3.11). These are used to update the head position parameters $\mathbf{p}_i$ in Eq. (3.12). Fig. 3.5 shows an example of applying this approach to signals measured with *Neuromag Vectorview*™ when a subject moved his head deliberately. When the subjects moves his head, the filter sometimes produces erroneous peaks, possibly due to muscle artifacts in the measurements, but converges quickly to the correct head position.

Correcting for head movements

By using the estimated head positions it is possible to compensate for the effect of the head movements. One way is to re-sample each response to represent magnetic fields measured in a reference head position. Publication P3 evaluates the minimum-norm estimate (MNE) correction that re-samples the measured fields using MNEs (Numminen et al., 1995). After the MNE-correction the averaging of the fields and other analysis can proceed using conventional methods.

Another approach evaluated in publication P3 is the forward calculation (FC) correction: the measured magnetic fields are not transformed, but instead effect of the head movements is taken into account when the magnetic field produced by the source models is calculated.

Properties of the correction methods considered in publication P3 are accuracy of the corrected estimates, increase in noise sensitivity caused by the correction methods, and calculation time needed for the methods. In simulation studies, the accuracy

of both correction methods is good, and in noiseless case both can be used to yield sufficiently accurate estimates even with large head movements.

The noise sensitivities of the two methods differ. Since the FC correction uses normal averages, the increase in noise sensitivity is negligible, while the MNE correction increased the noise sensitivity 30% in magnetic field alignment and 10% in dipole fitting.

Using the MNE correction involves a computationally heavy preprocessing phase where each individual response is separately transformed. The computational cost can be significantly reduced by using the signal-space correction described in (Uutela and Hämäläinen, 2001); unfortunately the noise sensitivity of this method is higher than that of the normal MNE correction. The FC correction needs no special preprocessing at all. The computational cost in source modeling is increased because of the corrected forward calculations, but the time is usually negligible compared to the preprocessing required by the MNE correction. If estimating parameters of the source model used involves a very high number of forward calculations, the FC correction may have a noticeable effect on the computation time. In these cases it is possible to simplify the calculations, instead of by using every head position separately, by using a weighted combinations of a few representative head positions that can be obtained, for example, with different clustering methods (Schalkoff, 1992).

Publication P3 included a test measurement where the head movements were measured during an auditory evoked response recording. The measurement contained three phases: one where the subject kept his head still and two were he moved his head deliberately. When the subject was keeping his head still, the results of the head position measurements were almost constant: the standard deviation of the estimated head positions was only 0.2 mm. When the subject was moving his head, the estimated head position changed with standard deviations of 6.2 and 7.5 mm. Since the successive head position measurements were independent, these results indicate that the proposed head position measurement is very sensitive.

These measurements do not rule out the possibility of biased measurements, but the conventional head position measurement has been verified during normal quality control of the system, and therefore a significant bias for this method is unlikely. During the actual head movements the estimation errors increase because the amplitudes change although they are assumed constant during the time window. If the estimate is calculated based on systems (3.11) and (3.12), errors can be decreased by using shorter time windows. However, during significant head movements the muscle artifacts can be strong, and therefore rejecting these responses from further analysis may be beneficial.

According to the simulation studies, the FC correction was accurate and noise tolerant. Also, it did not significantly increase the computational load. Therefore, in publication P3, FC correction was applied to correct the measurements with head movements. Fig. 3.6 shows that the corrected estimates are much closer to estimates obtained without head movements than the uncorrected estimates.
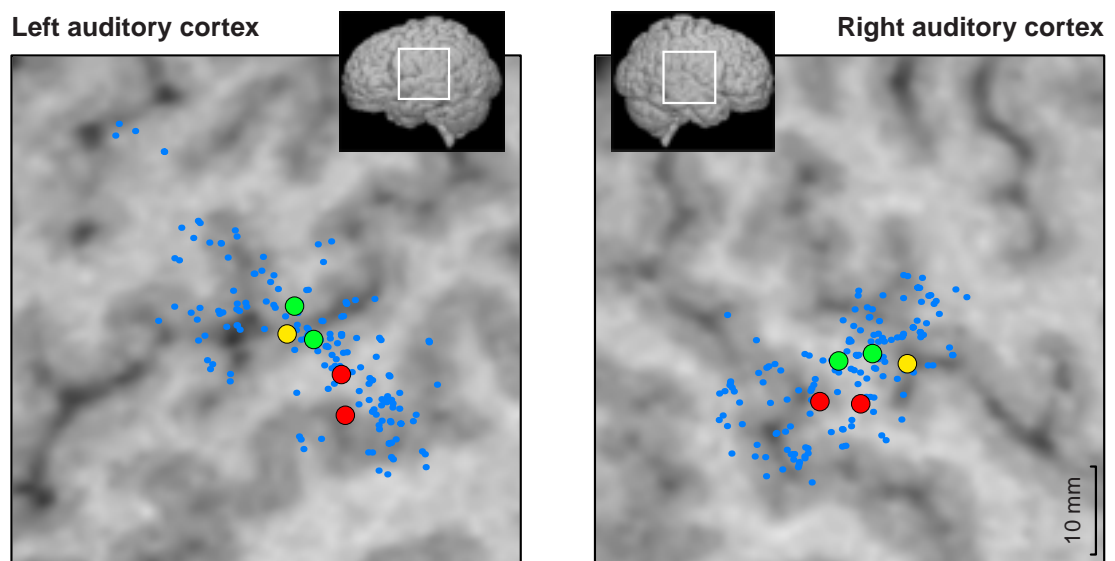
Figure 3.6:   Estimated source locations in the auditory cortices: one measurement when the head was kept still (yellow circles) and two measurements where the head was moved deliberately (red circles: conventional dipole model; green circles: dipole model with head movement correction). Blue dots depict the uncorrected dipole locations estimated with all the different head positions.

Chapter 4

Applications of the methods

4.1 Visuomotor interaction (P4)

The human brain has areas specialized in processing different sensory stimuli and to control movements. To perform motor acts in their surroundings, human beings have to incorporate the sensory information first processed at the sensory areas to the output from the motor areas. Publication P4 studies the interaction of visual and motor systems when the subjects follow a visually presented object with their eyes or finger.
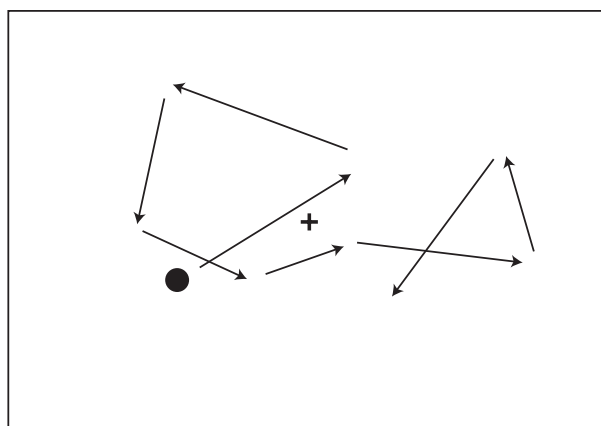

Figure 4.1: Schematic illustration of the path of the moving dot used as stimulation in the study of visuomotor interaction.

The subjects were watching a black dot that moved with a constant speed but changed the direction randomly after 0.3–2 s (Fig. 4.1). The subjects had three different tasks: in one block they watched the moving dot without moving their eyes from a fixation point (eye fixation task), in one block they followed the dot with their eyes (eye pursuit task), and in one block they mimicked the movements of the dot with their index finger (eye-finger pursuit task).

The neuromagnetic responses generated by the changes in the direction of the dot were measured with a *Neuromag-122*™. The digitized signals were averaged with respect to the direction changes and preprocessed to increase the signal-to-noise ratio. The results were analyzed with dipole modeling and, for the data of one subject, with MCE.

Different directional changes were averaged together. If the current orientation of the response depended on the direction, the different responses canceled each other, since the different directions were equally probable. The stimulus-related direction-

specific signals, including eye movement signals, were thus attenuated and the measurement was more sensitive to directionally non-specific brain signals.

Four bilateral brain areas were consistently activated: the lateral occipital area, the inferior and a superior parietal areas, and the frontal area. The occipital area was activated first, followed by the frontal and inferior parietal areas; superior parietal area was activated last. The strength of the occipital activation was independent of the subject's task, whereas the other areas, especially the inferior parietal, showed increasing activation with increasing visuomotor interaction. The results using dipole modeling and MCE were concordant.

It is likely that several areas in the occipital cortex are activated in this experiment and that the modeled occipital response may represent several of them. Based on their anatomical locations and behavior, the areas activated in the parietal and frontal cortices may correspond to areas found in experiments of the visual pathways in monkey brains (Van Essen et al., 1992). The most likely homologue of the superior and inferior parietal areas are the inferior parietal lobule areas 7a, associated with the spatial representation of the visual environment (Siegel and Read., 1997) and 7b, activated during hand movements (Hyvärinen and Poranen, 1974). The frontal area probably corresponds to frontal eye field (FEF) associated with planning and execution of saccades (Schall, 1997).

4.2   Visual attention (P5)

The resolution of human eyes is high only in a small part of the total visual field, and the attention keeps only few objects for detailed processing. However, the surroundings of a human change all the time. If an important, new object appears, it is crucial to attend to that and change the direction of the eyes as fast as possible.

The mechanisms for turning the eyes and shifting the attention have been previously studied both on monkeys and in humans (Corbetta, 1998). Both the parietal and frontal cortices are involved. The publication P5 studies in humans how the attention to a foveal target changes the processing of peripheral stimuli.

The experimental paradigm has been previously used to study the inferior parietal lobule in monkeys (Mountcastle et al., 1981). The attention of the subjects was targeted to a small, foveal square. When the center of the square lighted up, the subjects waited until the center dimmed and responded as fast as possible by lifting their finger (Fig. 4.2). A peripheral, large light rectangle was flashed both during the trial while the subjects were attending the square to notice its dimming and during the intertrial while the center of the square was dark and the subjects were waiting for the next trial. The experiment had also a session of passive watching, which had the same stimulus but no task.

Since there may be different attentional mechanisms, two control measurements were carried out. First we tested whether the effects were specific to visual attention by using a task requiring auditory attention. The visual stimulus was the same as in the main experiment, but instead of attending to the luminance changes in the center of the square, the subjects detected whether a 1–4 s tone ended in slight frequency modulation lasting 200 ms. The trial stimuli were presented during the tone was played and the intertrial stimuli during silence.

The second control experiment tested whether the effects were specific to the spatial target of attention. Peripheral visual stimuli were presented in eight possible lo-
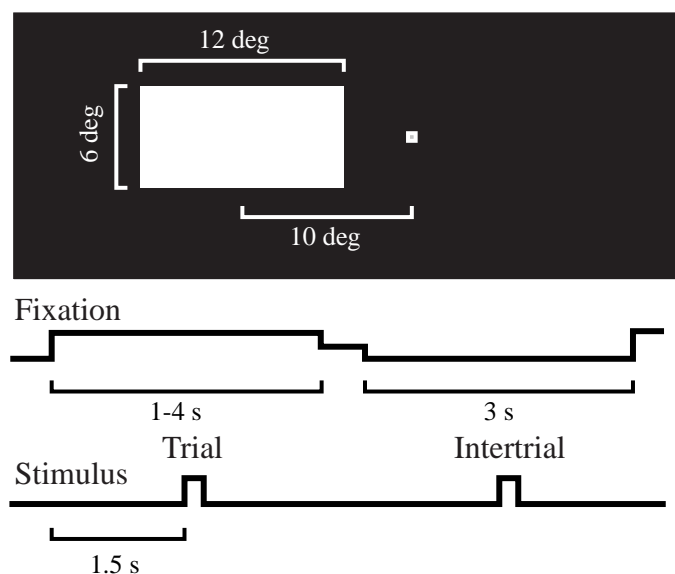
Figure 4.2: The experimental paradigm used in study of visual attention.

cations. First, a cue stimulus was presented, then 1–5 stimuli in different locations. When the cue stimulus was presented again, the subjects responded by lifting their finger. The responses to the attended and non-attended locations were studied separately.

Eleven subjects participated in the main experiment that was carried out with the *Neuromag-122*™. Two subjects participated in the control experiments one year after the main experiments; these measurements were carried out with the *Neuromag Vectorview*™. The source distribution was analyzed with MCE. The responses were studied individually, but to find out the most consistent responses over the subjects, also a group average was calculated by adding the MCEs of different subjects. The estimates were aligned based on anatomical locations on the surface of the head. Regions of interest were selected semi-manually and the attentional modulation was studied by comparing amplitudes in different cases.

Several sources were activated in different parts of the brain, but clear attentional modulation was observed in the frontal and parietal lobes. In a region of interest in the precentral area of the right hemisphere, the mean activation 100–160 ms after the stimulus was significantly stronger during trials than during the intertrials or passive watching. When responses of the subjects were studied separately, the area was clearly activated in 6/11 subjects; for all of them, the strongest activity occurred during the trial.

The activation in the parietal lobes showed more individual variability, but a posterior parietal area, clearly active in 8/11 subjects, was strongest during the trials in 4/8 cases. In all these cases, there was no clear activation in the prefrontal cortex, or it occurred only after the parietal activation. This suggests that the parietal and prefrontal area represent two alternative processing techniques.

Control measurements showed that the auditory attention did not produce the enhancement in the precentral area, but the peripheral visual attention did regardless of the spatial location of the attention. Thus, the effect is related to visual attention, not to general attentional level or to spatial attention.

Based on the anatomy, the prefrontal activation seems to correspond to the FEF;

Publi-cation	Left frontal			Right frontal			Left parietal			Right parietal		
	x	y	z	x	y	z	x	y	z	x	y	z
P4	−40	−4	42	45	−1	40	−38	−55	49	38	−55	50
							−60	−33	27	60	−37	26
P5	−37	−9	43	49	0	35	−44	−53	31	46	−50	40

Table 4.1: Centers of activated areas in publications P4 and P5. In P4, two different parietal areas were activated, while in P5, main differences were seen only in one. Coordinates are millimeters in the Talairach coordinate system that aligns the anatomy of the brains of the subjects with piecewise linear transformations (Talairach and Tournoux, 1988).

the estimated locations of the FEF area in publications P4 and P5 are close to each other (Table 4.1). The modulation of the activity in the parietal area corresponds to that in area 7a in monkeys. The locations of the parietal sources fall between the two parietal activated areas in publication P4.

4.3   Audiovisual integration (P6)

Objects have different properties that can be perceived using different senses. To be able to process the object as a whole, the information from different senses has to be combined (Stein and Meredith, 1993). In the brain, the information from different senses first has to converge to the same brain area. When the object is processed as a whole instead of the sum of the modality-specific properties, the specific processes have to interact. Publication P6 studied audiovisual integration using culturally learned objects, letters.

In the experiment, letters were presented to the subject visually by showing the characters and auditorily by playing the names of the letters. Audiovisual stimuli were presented as matching or different auditory and visual letter. Also meaningless control stimuli having similar auditory and visual properties as the main stimuli were presented. During the experiment, a matching letter and sound were presented first as a cue. The task of the subject was to lift his finger when the cue stimulus was presented either audiovisually or using one modality with no stimulus in the other modality.

Nine subjects were measured using the *Neuromag-122*™. The source distribution was estimated with MCE. The areas where the auditory and visual pathways converged were studied by generating an image of the minimum of the MCEs of unimodal auditory and visual responses. Because of the spatial uncertainty of the estimates, the MCEs were smoothed spatially. Because behavioral experiments have shown that the audiovisual integration can occur also with non-simultaneous stimuli, the MCEs were also smoothed temporally before taking the minimum. To extract the integration effects, the measured audiovisual magnetic responses and the sum of unimodal magnetic responses were subtracted. The integration effect was then studied both by spatial averaging and MCEs of the subtracted signals.

The responses were studied individually, but to find out the most consistent responses over the subjects, also a group average was calculated by adding the MCEs of different subjects. The estimates were aligned using piecewise linear transformation taking into account the anterior and posterior commissures and the size of the brain

(Talairach and Tournoux, 1988). Regions of interest were selected semi-manually.

The effect of the audiovisual integration was seen in the reaction times of the subjects; the reaction times for the audiovisual stimuli (425 ms) were clearly faster that those for the auditory (505 ms) or visual stimuli (520 ms) presented alone.

The early responses (60–120 ms) were stimulus-specific: the auditory stimulation activated mainly the temporal and the visual stimulation the occipital cortices. The early audiovisual responses were close to the sum of responses of unimodal stimuli, and the responses of letters and controls were similar.
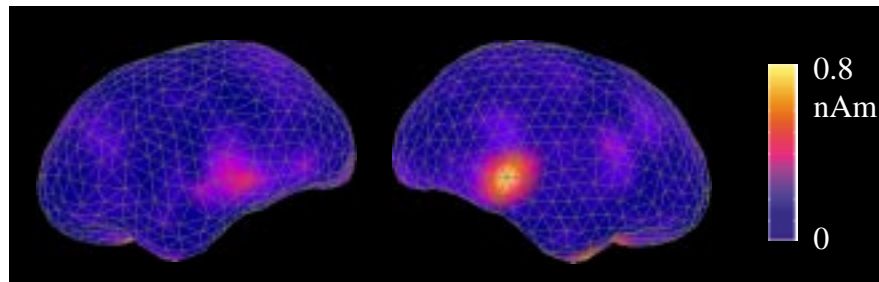

Figure 4.3: Brain areas showing audiovisual integration for letters. The group average shows strong interaction in the STS.

Convergence was detected in the temporal cortices around 200 ms after the stimulation. Following that, interaction was detected most consistently near superior temporal sulcus (STS) around 500 ms after the stimulus (Fig. 4.3). The current orientation calculated from the interaction field was opposite to that of the auditory and visual responses. Thus, the interaction was suppressive, *i.e.*, the audiovisual response was weaker than the sum of the unimodal responses. The interaction in the left STS also depended on the type of the stimulus: the interaction was strongest for matching letters, weaker for non-matching letters, and weakest for control stimuli. Interaction was detected also in some frontal and parietal areas, but it was weaker and did not show as clear stimulus dependence as in the left STS.

The convergence of audiovisual information on the left STS allows the area to learn to bind together different properties of the same object. Although most multisensory cells show multisensory potentiation, the population response in STS showed suppressive integration. This may reflect the fact that the different representations of the letter are culturally learned, and that the observed interaction may represent the processing of the same abstraction of the letter instead of the specific attributes.

4.4   Observing sign language (P7)

Sign languages are natural languages used mainly by deaf people. Instead of using sounds, the words and grammar are transmitted using hand gestures and facial expressions. Processing sign language involves some of the areas involved also in processing of auditory languages (Neville et al., 1998).

Publication P7 compared brain activation correlated with observing sign language in signers and non-signers. The signers automatically associated the signs with their semantic meaning; the non-signers could not even guess the meanings of the signs. Thus, the main differences between the groups was that the stimuli represented lan-

Experiment	Left STS			Right STS		
	x	y	z	x	y	z
Audiovisual integration	-53	-31	0	48	-31	6
Sign language	-56	-35	8	55	-31	14

Table 4.2: Centers of areas activated in the STS in publications P6 and P7.

guage to one group, and general movements to the other; another difference was that the signers had more experience in interpreting that kind of movements.

Videos representing signs in Finnish Sign Language were presented to the subjects. Each sign lasted 2–2.5 s with a still image between. Subjects were instructed to watch carefully the movements. Seven congenitally deaf, fluent users of the Finnish Sign Language and seven hearing, non-signing controls, were measured with *Neuromag-122*™. The responses were averaged in relation to the start of the movements for each sign. Due to hardware limitations, the jitter of the onset of the presented signs was about 200 ms, which diminished and spread possible fast onset responses.

The source distribution was analyzed with MCE. To study the strength and dynamics of activation in different areas, regions of interest were selected semi-manually for each subject. To compare the two groups, ROIs representing the coordinates and orientations for both subject groups were created. To produce unbiased estimates, the ROIs representing the same area were selected for both subject groups. Then, an average ROI was constructed by using the centers and orientations with smallest difference to those of the ROIs of both groups.

The measured magnetic field consisted of long, low frequency responses. Several brain areas were activated, including lateral occipital cortex close to the movement-sensitive visual area V5, inferior frontal cortex close to Broca's area, and the superior temporal sulcus. The same areas were activated mainly in similar ways for both subject groups although the activity was weaker for the signers in most brain areas. The clearest difference between the groups was the stronger activation of the right STS in signers.

Although the studies in publications P6 and P7 employed very different experimental paradigms, both demonstrated interesting language-related effects in activation of areas close to the STS. The activated areas in both hemispheres were about 1 cm from each other, the activation associated with viewing signs being slightly superior and lateral to the audiovisual interaction area of the letters (Table 4.2). They may be parts of the same functional, language related network.

One surprising finding in the results was the similarity of the activation within the classical language areas in the left inferior frontal cortex and STS regardless of whether the observed signs had a semantic meaning to the subject. The monkey premotor areas include mirror neurons that are active both during performing actions and observing them (Rizzolatti et al., 1996a) and the classical language areas in human brain show similar behavior (Rizzolatti et al., 1996b; Nishitani and Hari, 1999). Rizzolatti et al. (1996a) have proposed that the processes in the human brain used for language are related to the processes in monkey brains used for action recognition. This view is in concordance with the activation of the language areas also in the non-signing subjects.

Chapter 5

Conclusions

This work describes improvements in methods for estimating the activation of the brain generating neuromagnetic signals. Two publications describe new ways of using different source models: Publication P1 discusses ways for using over-determined multi-dipole models without knowing approximate source locations in advance. Publication P2 discusses an under-determined, distributed current estimate that uses assumptions suitable for MEG studies. Publication P3 studies methods for increasing the accuracy of the estimates if the subject moves during the measurements. The proposed method can be used together with different source models.

All the methods have been developed to be practical, *i.e.*, they work with realistic, noisy measurements and that they do not require excessive computing power. The estimation methods are also planned to be more automatic and work with the same assumptions in different measurements.

Of the two developed estimation methods, the MCE has been widely used but multidipole modeling with global optimization not very much yet. One reason is that the global optimization methods have not been implemented in user friendly MEG analysis software, but also that the MCE offers more novel possibilities. The head movement correction method is rather new; it is not yet added to existing measurement and analysis software, but studies applying the method are under way.

The applications in this work demonstrate different uses of the MCE. Publication P4 uses MCE to validate dipole modeling. The other publications used MCE to analyze complicated responses that might have been difficult to model using dipoles. They also employed the general spatial representation offered by MCE to combine different measurements together. All three experimental studies used MCE to combine results from different subjects to group averages, but also to perform specific comparisons: P5 used MCE to compare the activations during different tasks in same subjects, P6 used MCEs of different tasks to estimate convergence and interaction, and P7 used MCE to compare activations during similar tasks in two subject groups.

When different brain imaging modalities become more common, it becomes more viable to combine information from different types of measurements. When distributed current estimates are used, information from fMRI or PET can be used as *a priori* information for the estimate (Dale and Sereno, 1993; Dale et al., 2000); this approach is also directly applicable with MCE (Uutela and Ryymin, 1999). The methods developed in this work are one step towards robust and automatic analysis methods for neuromagnetic measurements.

Bibliography

Ahlfors, S. and Ilmoniemi, R. (1989). Magnetometer position indicator for multichannel MEG. In *Proceedings of the 7th International Conference on Biomagnetism*, pages 693–696.

Ahonen, A. I., Hämäläinen, M. S., Kajola, M. J., Knuutila, J. E. T., Laine, P. P., Lounasmaa, O. V., Parkkonen, L. T., Simola, J. T., and Tesche, C. D. (1993). A 122-channel SQUID instrument for investigating the magnetic signals from the human brain. *Physica Scripta*, T49:198–205.

Backus, G. and Gilbert, F. (1970). Uniqueness in the inversion of inaccurate gross earth data. *Phil. Trans. R. Soc.*, 266:123–192.

Barnard, A., Duck, I., and Lynn, M. (1967). The application of electromagnetic theory to electrocardiology. I. Derivation of the integral equations. *Biophys. J.*, 7:443–462.

Barth, D., Sutherling, W., Engel, J., and Beatty, J. (1982). Neuromagnetic localization of epileptiform spike activity in the human brain. *Science*, 218:891–894.

Berkelaar, M. (2001). Mixed integer linear program solver lp_solve. <ftp://ftp.es.ele.tue.nl/pub/lp_solve/>. October 22.

Beucker, R. and Schlitt, H. (1996). On minimal l_p-norm solutions of the biomagnetic inverse problem. *IEEE Trans. Biomed. Eng.* Submitted.

Beucker, R. and Schlitt, H. (1997). Spatial and temporal prewhitening of multi-channel EEG/MEG data. *Brain Topography*, 10:168–169.

Brenner, D., Lipton, J., Kaufman, L., and Williamson, S. J. (1978). Somatically evoked magnetic fields of the human brain. *Science*, 199:81–83.

Brenner, D., Williamson, S. J., and Kaufman, L. (1975). Visually evoked magnetic fields of the human brain. *Science*, 190:480–482.

Buchner, H., Knoll, G., Fuchs, M., Rienacker, A., Beckmann, R., Wagner, M., Silny, J., and Pesch, J. (1997). Inverse localization of electric dipole current sources in finite element models of the human head. *Electroenceph. Clin. Neurophysiol.*, 102:267–278.

Buchner, H., Waberski, T., Fuchs, M., Wischmann, H.-A., Wagner, M., and Drenckhahn, R. (1995). Comparison of realistically shaped boundary-element and spherical head models in source localization of early somatosensory evoked potentials. *Brain Topography*, 8:137–143.

Cohen, D. (1968). Magnetoencephalography: Evidence of magnetic fields produced by alpha-rhythm currents. *Science*, 161:784–786.

Corbetta, M. (1998). Frontoparietal cortical networks for directing attention and the eye to visual locations: Identical, independent, or overlapping neural systems? *Proc. Natl. Acad. Sci. USA*, 95:831–838.

Corona, A., Marchesi, M., Martini, C., and Ridella, S. (1987). Minimizing multimodal functions of continuous variables with the "simulated annealing" algorithm. *ACM Transactions on Mathematical Software*, 13:262–280.

Dale, A., Fischl, B., and Sereno, M. (1999). Cortical surface-based analysis I. Segmentation and surface reconstruction. *NeuroImage*, 9:179–194.

Dale, A., Liu, A., Fischl, B., Buckner, R., Belliveau, J., Lewine, J., and Halgren, E. (2000). Dynamic statistical parametric mapping: Combining fMRI and MEG for high-resolution imaging of cortical activity. *Neuron*, 26:55–67.

Dale, A. and Sereno, M. (1993). Improved localization of cortical activity by combining EEG and MEG with MRI cortical surface reconstruction: A linear approach. *J. Cogn. Neurosci.*, 5:162–176.

de Munck, J., Verbunt, J., van 't Ent, D., and van Dijk, B. (2001). The use of an MEG device as a 3D digitizer and a motion correction system. In Nenonen, J., Ilmoniemi, R. J., and Katila, T., editors, *Biomag 2000, Proceedings of the 12th International Conference on Biomagnetism*, pages 801–804.

de Munck, J., Vijn, P., and Lopes da Silva, F. (1992). A random dipole model for spontaneous brain activity. *IEEE Trans. Biomed. Eng.*, 39:791–804.

Erné, S. N., Narici, L., Pizzella, V., and Romani, G. L. (1987). The positioning problem in biomagnetic measurements: A solution for arrays of superconducting sensors. *IEEE Trans. Magn.*, MAG-23:1319–1322.

Friston, K. J., Holmes, A. P., Worsley, K. J., Poline, J.-P., Frith, C. D., and Frackowiack, R. S. J. (1995). Statistical parametric maps in functional imaging: A general linear approach. *Hum. Brain Mapp.*, 2:189–210.

Fuchs, M., Wagner, M., Kohler, T., and Wischmann, H.-A. (1999). Linear and nonlinear current density reconstructions. *J. Clin. Neurophysiol.*, 16:267–295.

Fuchs, M., Wischmann, H.-A., Wagner, M., and Krüger, J. (1995). Coordinate system matching for neuromagnetic and morphological reconstruction overlay. *IEEE Trans. Biomed. Eng.*, 42:416–420.

Gallen, C., Sobel, D., Waltz, T., Aung, M., Copeland, B., Schwartz, B., Hirschkoff, E., and Bloom, F. (1993). Noninvasive presurgical neuromagnetic mapping of somatosensory cortex. *Neurosurgery*, 33:260–268.

Gauss, C. F. (1863). Theoria motus corporum coelestium in sectionibus conicis Solem ambientium. In *Gauss Werke Band VII. Theoretische Astronomie*, pages 1–288. Dietrich, Göttingen. First publication 1809.

Gelman, A., Carlin, J. B., Stern, H. S., and Rubin, D. B. (1995). *Bayesian data analysis*. Chapman and Hall.

Gerson, J., Vardenas, V. A., and Fein, G. (1994). Equivalent dipole parameter estimation using simulated annealing. *Electroenceph. Clin. Neurophysiol.*, 92:161–168.

Geselowitz, D. B. (1967). On bioelectric potentials in an inhomogeneous volume conductor. *Biophys. J.*, 7:1–11.

Geselowitz, D. B. (1970). On the magnetic field generated outside an inhomogeneous volume conductor by internal current sources. *IEEE Trans. Magn.*, 6:346–347.

Gilbert, C. D., Das, A., Ito, M., Kapadia, M., and Westheimer, G. (1996). Spatial integration and cortical dynamics. *Proc. Natl. Acad. Sci. USA*, 93:615–622.

Gorodnitsky, I., George, J., and Rao, B. (1995). Neuromagnetic source imaging with FOCUSS: a recursive weighted minimum norm algorithm. *Electroenceph. Clin. Neurophysiol.*, 95:231–251.

Gross, J. and Ioannides, A. (1999). Linear transformations of data space in MEG. *Phys. Med. Biol.*, 44:2081–2097.

Gross, J., Kujala, J., Hämäläinen, M., Timmermann, L., Schnitzler, A., and Salmelin, R. (2001). Dynamic imaging of coherent sources: Studying neural interactions in the human brain. *Proc. Natl. Acad. Sci. USA*, 98:694–699.

Halgren, E., Raij, T., Marinkovic, K., Jousmäki, V., and Hari, R. (2000). Cognitive response profile of the human fusiform face area as determined by MEG. *Cerebral Cortex*, 10:69–81.

Hämäläinen, M. S., Hari, R., Ilmoniemi, R. J., Knuutila, J., and Lounasmaa, O. V. (1993). Magnetoencephalography — theory, instrumentation, and applications to noninvasive studies of the working human brain. *Rev. Mod. Phys.*, 65:413–497.

Hämäläinen, M. S. and Ilmoniemi, R. J. (1984). Interpreting measured magnetic fields of the brain: Estimates of current distributions. Technical Report TKK-F-A559, Helsinki University of Technology.

Hämäläinen, M. S. and Ilmoniemi, R. J. (1994). Interpreting magnetic fields of the brain: minimum norm estimates. *Med. & Biol. Eng. & Comput.*, 32:35–42.

Hämäläinen, M. S. and Sarvas, J. (1989). Realistic conductivity geometry model of the human head for interpretation of neuromagnetic data. *IEEE Trans. Biomed. Eng.*, 36:165–171.

Hamilton, W. (1847). On quaternions. *Proc. Roy. Irish. Acad.*, 3:1–16.

Haneishi, H., Ohyama, N., Sekihara, K., and Honda, T. (1994). Multiple current dipole estimation using simulated annealing. *IEEE Trans. Biomed. Eng.*, 41:1004–1009.

Hari, R., Aittoniemi, K., Järvinen, M.-L., Katila, T., and Varpula, T. (1980). Auditory evoked transient and sustained magnetic fields of the human brain: Localization of neural generators. *Exp. Brain Res.*, 40:237–240.

Hari, R., Joutsiniemi, S.-L., and Sarvas, J. (1988). Spatial resolution of neuromagnetic records: theoretical calculations in a spherical model. *Electroenceph. Clin. Neurophysiol.*, 71:64–72.

Hari, R., Kaukoranta, E., Reinikainen, K., Huopaniemi, T., and Mauno, J. (1983). Neuromagnetic localization of cortical activity evoked by painful dental stimulation in man. *Neurosci. Lett.*, 42:77–82.

Helmholtz, H. (1853). Ueber einige Gesetze der Vertheilung elektrischer Ströme in körperlichen Leitern, mit Anwendung auf die thierisch-elektrischen Versuche. *Ann. Phys. Chem.*, 89:211–233, 353–377.

Holland, J. H. (1975). *Adaptation in Natural and Artificial Systems*. University of Michigan.

Huang, M., Aine, C., Supek, S., Best, E., Ranken, D., and Flynn, E. (1998). Multi-start downhill simplex method for spatio-temporal source localization in magnetoencephalography. *Electroenceph. Clin. Neurophysiol.*, 108:32–44.

Hyvärinen, J. and Poranen, A. (1974). Function of parietal associative area 7 as revealed from cellular discharges in alert monkeys. *Brain*, 97:673–692.

Incardona, F., Narici, L., and Modena, I. (1992). Three-dimensional localization system for small magnetic dipoles. *Rev. Sci. Instrum.*, 63:4161–4166.

Ioannides, A., Bolton, J., and Clarke, C. (1990). Continuous probabilistic solutions to the biomagnetic inverse problem. *Inverse Problems*, 6:523–542.

Iversen, L. L. (1979). The chemistry of the brain. *Sci. Am.*, 241:118–129.

Jazwinski, A. (1970). *Stochastic Processes and Filtering*. Academic Press, New York.

Johnson, C. R. (1997). Computational and numerical methods for bioelectric field problems. *Crit. Rev. in Biomed. Eng.*, 25:1–81.

Josephson, B. D. (1962). Possible new effects in superconductive tunneling. *Phys. Lett.*, 1:251–253.

Jousmäki, V. and Hari, R. (1996). Cardiac artifacts in magnetoencephalogram. *J. Clin. Neurophysiol.*, 13:172–176.

Kalman, R. (1960). A new approach to linear filtering and prediction problems. *ASME J. Basic Eng.*, 82:35–45.

Kandel, E. R., Schwartz, J. H., and Jessell, T. M. (1991). *Principles of Neural Science*. Elsevier, 3rd edition.

Kettenmann, B., Jousmäki, V., Portin, K., Salmelin, R., Kobal, G., and Hari, R. (1996). Odorants activate the human superior temporal sulcus. *Neurosci. Lett.*, 203:143–145.

Kirkpatrick, K., Gelatt, Jr., C. D., and Vecchi, M. P. (1983). Optimization by simulated annealing. *Science*, 220:671–680.

Knuutila, J., Ahonen, A. I., Hämäläinen, M. S., Ilmoniemi, R. J., and Kajola, M. J. (1985). Design considerations for multichannel SQUID magnetometers. In Hahlbohm, H. D. and Lübbig, H., editors, *SQUID'85: Superconducting Quantum Interference Devices and their Applications*, pages 939–944, Berlin. Walter de Gruyter.

Leahy, R., Jeffs, B., and Wu, Z. (1988). A nonlinear simplex algorithm for minimum order solutions. In *Proc. IEEE ICASSP*, volume 2, pages 745–748.

Lewine, J., Andrews, R., Chez, M., Patil, A., Devinsky, O., Smith, M., Kanner, A., Davis, J., Funke, M., Jones, G., Chong, B., Provencal, S., Weisend, M., Lee, R., and Orrison, Jr., W. (1999). Magnetoencephalographic patterns of epileptiform activity in children with regressive autism spectrum disorders. *Pediatrics*, 104:405–418.

Lötjönen, J., Reissman, P., Magnin, I., and Katila, T. (1999). Model extraction from magnetic resonance volume data using the deformable pyramid. *Med. Image Anal.*, 3:387–406.

Lütkenhöner, B. (1998). Dipole separability in a neuromagnetic source analysis. *IEEE Trans. Biomed. Eng.*, 45:572–581.

Mäkelä, J. P., Kirveskari, E., Seppä, M., Hämäläinen, M., Forss, N., Avikainen, S., Salonen, O., Salenius, S., Kovala, T., Randell, T., Jääskeläinen, J., and Hari, R. (2001). Three-dimensional integration of brain anatomy and function to facilitate intraoperative navigation around the sensorimotor strip. *Hum. Brain Mapp.*, 12:180–192.

Malmivuo, J. (1976). *On the Detection of the Magnetic Heart Vector — An Application of the Reciprocity Theorem*. Acta Polytechnica Scandinavica, Electrical Engineering Series No. 39. The Finnish Academy of Technical Sciences, Helsinki. Ph.D. Thesis.

Matsuura, K. and Okabe, U. (1995). Selective minimum-norm solution of the biomagnetic inverse problem. *IEEE Trans. Biomed. Eng.*, 42:608–615.

Matsuura, K. and Okabe, U. (1997). A robust reconstruction of sparse biomagnetic sources. *IEEE Trans. Biomed. Eng.*, 44:720–726.

Metropolis, N., Rosenbluth, A. W., Rosenbluth, M. N., Teller, A. H., and Teller, E. (1953). Equation of state calculation by fast computing machines. *J. Chem. Phys.*, 21:1087–1092.

Mosher, J. and Leahy, R. (1998). Recursive MUSIC: a framework for EEG and MEG source localization. *IEEE Trans. Biomed. Eng.*, 45:1342–1354.

Mosher, J. C., Lewis, P. S., and Leahy, R. M. (1992). Multiple dipole modeling and localization from spatio-temporal MEG data. *IEEE Trans. Biomed. Eng.*, 39:541–557.

Mountcastle, V. B., Andersen, R. A., and Motter, B. C. (1981). The influence of attentive fixation upon the excitability of light-sensitive neurons of the posterior parietal cortex. *J. Neurosci.*, 7:1218–1235.

Näätänen, R., Lehtokoski, A., Lennes, M., Cheour, M., Huotilainen, M., Iivonen, A., Vainio, M., Alku, P., Ilmoniemi, R., Luuk, A., J, A., Sinkkonen, J., and Alho, K. (1997). Language-specific phoneme representations revealed by electric and magnetic brain responses. *Nature*, 385:432–434.

Narici, L., Portin, K., Salmelin, R., and Hari, R. (1998). Responsiveness of human cortical activity to rhythmical stimulation: a three-modality, whole-cortex neuromagnetic investigation. *NeuroImage*, 7:209–223.

Nenonen, J. (1994). Solving the inverse problem in magnetocardiography. *IEEE Eng. Med. Biol. Mag.*, 13:487–496.

Nenonen, J., Ilmoniemi, R. J., and Katila, T., editors (2001). *Biomag 2000, Proceedings of the 12th International Conference on Biomagnetism*, Espoo, Finland.

Neville, H. J., Bavelier, D., Corina, D., Rauschecker, J., Karni, A., Lalwani, A., Braun, A., Clark, V., Jezzard, P., and Turner, R. (1998). Cerebral organization for language in deaf and hearing subjects: Biological constraints and effects of experience. *Proc. Natl. Acad. Sci. USA*, 95:922–929.

Nishitani, N. and Hari, R. (1999). Temporal dynamics of cortical representation for action. *Proc. Natl. Acad. Sci. USA*, 97:913–918.

Nolte, G. and Curio, G. (1999). Unbiased estimates of spatial source extent using multipole modeling of MEG data: a theoretical analysis. In Yoshimoto, T., Kotani, M., Kuriki, S., Karibe, H., and Nakasato, N., editors, *Recent Advances in Biomagnetism: Proceedings of the 11th International Conference on Biomagnetism*, pages 282–285, Sendai, Japan. Tohoku University Press.

Numminen, J., Ahlfors, S., Ilmoniemi, R., Montonen, J., and Nenonen, J. (1995). Transformation of multichannel magnetocardiographic signals to standard grid form. *IEEE Trans. Biomed. Eng.*, 42:72–77.

Orchard-Hays, W. (1968). *Advanced Linear-programming Computing Techniques*. McGraw-Hill.

Paetau, R., Kajola, M., and Hari, R. (1990). Magnetoencephalography in the study of epilepsy. *Neurophysiol. Clin.*, 20:169–187.

Pascual-Marqui, R. D., Michel, C. M., and Lehmann, D. (1994). Low-resolution electromagnetic tomography: A new method for localizing electrical activity in the brain. *Int. J. Psychophysiol.*, 18:49–65.

Ramon, C., Wang, Y., Haueisen, J., Schimpf, P., Jaruvatanadilok, S., and Ishimaru, A. (2000). Effect of myocardial anisotropy on the torso current flow patterns, potentials and magnetic fields. *Phys. Med. Biol.*, 45:1141–1150.

Rizzolatti, G., Fadiga, L., Gallese, V., and Fogassi, L. (1996a). Premotor cortex and the recognition of motor actions. *Cognit. Brain Res.*, 3:131–141.

Rizzolatti, G., Fadiga, L., Matelli, M., Bettinardi, V., Paulesu, E., Perani, D., and Fazio, F. (1996b). Localization of grasp representations in humans by PET: 1. Observation versus execution. *Exp. Brain Res.*, 111:246–252.

Robinson, S. (1989). Theory and practice of lead fiel synthesis analysis. In Williamson, S. J., Hoke, M., Stroink, G., and Kotani, M., editors, *Advances in Biomagnetism*, pages 599–602. Plenum.

Salenius, S., Portin, K., Kajola, M., Salmelin, R., and Hari, R. (1997). Cortical control of human motoneuron firing during isometric contraction. *J. Neurophysiol.*, 77:3401–3405.

Salmelin, R., Hari, R., Lounasmaa, O. V., and Sams, M. (1994). Dynamics of brain activation during picture naming. *Nature*, 368:463–465.

Salmelin, R., Service, E., Kiesilä, P., Uutela, K., and Salonen, O. (1996). Impaired perception of visual word form in dyslexia revealed with magnetoencephalography. *Annals of Neurology*, 40:157–162.

Sarvas, J. (1987). Basic mathematical and electromagnetic concepts of the biomagnetic inverse problem. *Phys. Med. Biol.*, 32:11–22.

Schalkoff, R. (1992). *Pattern Recognition: Statistical, Structural and Neural Approaches*. John Wiley & Sons, Inc.

Schall, J. D. (1997). Visuomotor areas of the frontal lobe. In Rockland, K. S., Kaas, J. H., and Peters, A., editors, *Extrastriate Cortex in Primates*, volume 12 of *Cerebral Cortex*, pages 527–638. Plenum.

Scherg, M. (1990). Fundamentals of dipole source potential analysis. In Grandori, F., Hoke, M., and Romani, G. L., editors, *Auditory Evoked Magnetic Fields and Electric Potentials*, pages 40–69. Karger, Basel. Vol. 6 of *Advances in Audiology*.

Schmidt, D. M., George, J. S., and Wood, C. C. (1999). Bayesian inference applied to the electromagnetic inverse problem. *Hum. Brain Mapp.*, 7:195–212.

Schmidt, R. (1986). Multiple emitter location and signal parameter estimation. *IEEE Trans. Antennas Propag.*, AP-34:276–280.

Schormann, T., Henn, S., and Zilles, K. (1996). A new approach to fast elastic alignment with application to human brains. In Kikinis, R. and Hoehne, K. H., editors, *Visualization in Biomedical Computing. Proceedings.*, number 1131 in Lecture Notes Comput. Sci., pages 337–342.

Sekihara, K., Nagarajan, S., Poeppel, D., Marantz, A., and Miyashita, Y. (2001). Reconstructing spatio-temporal activities of neural sources using an MEG vector beamformer technique. *IEEE Trans. Biomed. Eng.*, 48:760–771.

Sekihara, K., Poeppel, D., Marantz, A., Koizumi, H., and Miyashita, Y. (1997). Noise covariance incorporated MEG-MUSIC algorithm: a method for multiple-dipole estimation tolerant of the influence of background brain activity. *IEEE Trans. Biomed. Eng.*, 44:839–847.

Seppä, M. (1997). 3D processing of magnetic resonance images in neuromagnetic studies. Master's thesis, Helsinki University of Technology. In Finnish.

Seppä, M. and Hämäläinen, M. (2000). MEG source visualization with texture-mapped triangle meshes. In *Book of Abstracts, 12th International Conference on Biomagnetism*, page 186, Helsinki University of Technology, Finland.

Siegel, R. M. and Read., H. L. (1997). Construction and representation of visual space in the inferior parietal lobule. In Rockland, K. S., Kaas, J. H., and Peters, A., editors, *Extrastriate Cortex in Primates*, volume 12 of *Cerebral Cortex*, pages 499–525. Plenum.

Singh, K. D., Holliday, I. E., Furlong, P. L., and Harding, G. F. A. (1997). Evaluation of MRI-MEG/EEG co-registration strategies using Monte Carlo simulation. *Electroenceph. Clin. Neurophysiol.*, 102:81–85.

Sorenson, H. W. (1980). *Parameter estimation : principles and problems*. Number 9 in Control and systems theory. Dekker.

Stein, B. E. and Meredith, M. A. (1993). *The Merging of the Senses*. MIT Press.

Talairach, J. and Tournoux, P. (1988). *Co-Planar Stereotaxic Atlas of the Human Brain*. Thieme Medical Publishers, New York.

Tarantola, A. (1987). *Inverse Problem Theory*. Elsevier.

Tarkiainen, A. (1997). Confidence regions of the current-dipole model in magnetoencephalography. Master's thesis, Helsinki University of Technology. In Finnish.

Tiihonen, J., Kajola, M., and Hari, R. (1989). Magnetic mu rhythm in man. *Neurosci.*, 32:793–800.

Tikhonov, A. N. and Arsenin, V. Y. (1977). *Solutions of Ill-Posed Problems*. Scripta Series in Mathematics. John Wiley.

Törn, A. and Zhilinskas, A. (1989). *Global Optimization*. Number 350 in Lecture Notes in Computer Science. Springer-Verlag.

Tripp, J. H. (1983). Physical concepts and mathematical models. In Williamson, S. J., Romani, G.-L., Kaufman, L., and Modena, I., editors, *Biomagnetism: An Interdisciplinary Approach*, pages 101–139. Plenum.

Tuomisto, T., Hari, R., Katila, T., Poutanen, T., and Varpula, T. (1983). Studies of auditory evoked magnetic and electric responses: Modality specificity and modelling. *Il Nuovo Cimento*, 2D:471–483.

Uusitalo, M. and Ilmoniemi, R. (1997). Signal-space projection method for separating MEG or EEG into components. *Med. & Biol. Eng. & Comput.*, 35:135–140.

Uutela, K. and Hämäläinen, M. (2001). Correcting for head movements in MEG inverse problem. In Nenonen, J., Ilmoniemi, R. J., and Katila, T., editors, *Biomag 2000, Proceedings of the 12th International Conference on Biomagnetism*, pages 809–812.

Uutela, K. and Ryymin, P. (1999). Combined analysis of MEG and fMRI using minimum l^1-norm estimates. In Yoshimoto, T., Kotani, M., Kuriki, S., Karibe, H., and Nakasato, N., editors, *Recent Advances in Biomagnetism: Proceedings of the 11th International Conference on Biomagnetism*, pages 933–936, Sendai, Japan. Tohoku University Press.

Van Essen, D. C., Anderson, C. H., and Felleman, D. J. (1992). Information-processing in the primate visual system: an integrated systems perceptive. *Science*, 255:419–423.

Vigário, R., Särelä, J., Jousmäki, V., Hämäläinen, M., and Oja, E. (2000). Independent component approach to the analysis of EEG and MEG recordings. *IEEE Trans. Biomed. Eng.*, 47:589–593.

Williamson, S. J., Wang, J.-Z., and Ilmoniemi, R. J. (1989). Method for locating sources of human alpha activity. In Williamson, S. J., Hoke, M., Stroink, G., and Kotani, M., editors, *Advances in Biomagnetism*, pages 257–260, New York. Plenum.

Yoshimoto, T., Kotani, M., Kuriki, S., Karibe, H., and Nakasato, N., editors (1999). *Recent Advances in Biomagnetism: Proceedings of the 11th International Conference on Biomagnetism*, Sendai, Japan. Tohoku University Press.

Zimmerman, J. E., Thiene, P., and Harding, J. T. (1970). Design and operation of stable rf-biased superconducting point-contact quantum devices and a note on the properties of perfectly clean metal contacts. *J. Appl. Phys.*, 41:1572–1580.